



Mid- to Late Neoproterozoic Development and Provenance of the Adelaide Superbasin

Jarred C. Lloyd *^{1,2}, Alan S. Collins ³, Morgan L. Blades ¹, Sarah E. Gilbert ³, Jacob A. Mulder ¹, Kathryn J. Amos ¹

¹School of Physics, Chemistry and Earth Sciences, The University of Adelaide, Adelaide, SA 5005, Australia | ²Department for Energy and Mining, Geological Survey of South Australia, Adelaide SA 5000, Australia | ³Mineral Exploration Cooperative Research Centre, School of Physics, Chemistry and Earth Sciences, The University of Adelaide, Adelaide, SA 5005, Australia | ⁴Adelaide Microscopy, The University of Adelaide, Adelaide, SA 5005, Australia

Abstract Late Tonian sequences of the Adelaide Superbasin were witness to the birth of the proto-Pacific Ocean during the breakup of Rodinia. Understanding the sedimentology and provenance of these rocks from across the basin is key to understanding their deposition over c. 70 million years, the local palaeogeography, and leads to a better understanding of the early development of the proto-Pacific Ocean. While the sedimentology of the Burra Group is well studied in most areas, provenance studies on these sequences using detrital zircon have been limited in scope and lack both spatial and temporal diversity. We begin to address this knowledge gap. Samples were taken from across the Adelaide Superbasin to understand both spatial and temporal related changes in provenance. Our findings highlight the necessity of this approach by uncovering both subtle, and abrupt significant changes in detrital zircon spectra for coeval samples from across the basin, and up-sequence in local areas. Our results highlight significant changes in provenance c. 790 Ma in the north of the basin, and c. 740 Ma in the south of the basin. This suggests a southward advancement of the rift basin, gradually opening to southerly sediment supply. We posit the existence of an unrecognised source of c. 1000–900 Ma zircon to the north or northeast of the basin to account for latest Stenian to earliest Tonian detrital zircon in the Myrtle Springs Formation. Additionally, we explore the comparison of coeval Tasmanian and Laurentian sequences, suggesting a stronger Australia-Tasmania link than Tasmania-Laurentia as time progresses.

Executive Editor:
R. da Silva Schmitt
Technical Editor:
Mohamed Gouiza

Reviewers:
Peter Cawood
Mauro Geraldés

Submitted:
16 August 2023
Accepted:
14 August 2024
Published:
2 September 2024

1 Introduction

The mid (c. 850 Ma) to late (c. 720 Ma) Tonian (1000–720 Ma) was a critical time in Earth's history. The breakup of the supercontinent Rodinia (Figure 1) was well underway (Li *et al.*, 2008; Merdith *et al.*, 2017), numerous large igneous provinces were emplaced (Ernst *et al.*, 2008), and the climate began to show hints of the oncoming global glaciations of the Cryogenian (MacLennan *et al.*, 2020). The record of this time is preserved in the many Tonian palaeo-rift sequences found globally (Merdith *et al.*, 2019). The South Australian Adelaide Superbasin (Lloyd *et al.*, 2020) (Figures 2 and 3) is one of the largest of these and contains an extensive and well preserved Tonian succession. The primary rift sequences in the superbasin, the Callanna and Burra groups, are key to understanding the evolution of the rift system and the basin's position within Rodinia as they formed during the initial stages of rifting when the superbasin was most likely to have

had connection to its paleogeographic counterpart (e.g. Laurentia). Compressive tectonic stresses (Foden *et al.*, 2006, 2020; Hall, 2018; Lubiniecki *et al.*, 2020; Mackay, 2011) have folded, uplifted and dismembered the sequences of the superbasin, and salt tectonics has significantly influenced the later depositional sequences (Heysen Supergroup, Moralana Supergroup) and disrupted many of the early rift sequences in the process (Counts *et al.*, 2019; Mackay, 2011; Mount, 1976; Rowan *et al.*, 2020). These factors, along with the vast size and the effects of hundreds of millions of years of time since deposition, have obscured the nuanced evolution of the superbasin. Despite this, numerous prior studies have made great advances on understanding the evolution of the basin (e.g. Armistead *et al.*, 2020; Betts *et al.*, 2018; Counts and Amos, 2016; Howchin, 1904; Jago *et al.*, 2018; Keeman *et al.*, 2020; Lechte and Wallace, 2015; Lloyd *et al.*, 2020, 2022, 2023; Mackay, 2011; Mancktelow, 1979; Mawson, 1947; Mawson and Sprigg, 1950; Mount, 1976; Murrell, 1977; Preiss, 1987, 2000; Rose *et al.*, 2013; Sprigg, 1952; Stüeken *et al.*, 2019; Toteff, 1977; Uppil, 1980; Virgo *et al.*, 2021, 2023;

*✉ jarred.lloyd@adelaide.edu.au

Williams et al., 2008).

Until recently, detrital provenance studies (Keeman et al., 2020; Lloyd et al., 2020), were limited in scale (Ireland et al., 1998; Job, 2011; Shahin, 2016), or specifically targeted (Rose et al., 2013). Detrital zircon (DZ) U–Pb age studies provide supplementary, but particularly useful insight about the palaeo-tectonic/geographic evolution of a basin through time by investigating changes in source of robust detrital material. To date, limited, or very targeted U–Pb DZ data exist (Keeman et al., 2020; Lloyd et al., 2020; Van der Wolff, 2020) for the Burra Group, with key sequences (e.g. the Myrtle Springs Formation) having no data.

Here we present U–Pb DZ data from the Burra Group, with additional, limited, data from the Yerelina Subgroup (representing the Marinoan/Elatina Glaciation) and Pound Subgroup (the uppermost sequences of the Adelaide Rift Complex). Due to the extensive literature available on the Yerelina and Pound subgroups (e.g. Counts and Amos, 2016; Counts et al., 2016; Le Heron et al., 2011; Lechte and Wallace, 2015; Lloyd et al., 2020; Preiss, 1993, 2000; Rose et al., 2013; Williams et al., 2008), and limited U–Pb DZ data presented for those subgroups in this study, we primarily focus on the provenance and evolution of the Burra Group. Notably, this study presents the first U–Pb DZ data that compares upper Emeroo Subgroup time equivalent sequences across the North Flinders Ranges (east–west) and additionally lays the framework for better understanding the north–south evolution of the basin during Burra Group deposition. However, we use the additional data, and data from previous studies (e.g. Keeman et al., 2020; Lloyd et al., 2020, 2022, 2023) to explore the Australia-Tasmania-Laurentia (Figure 1).

2 Geological Background

2.1 Adelaide Superbasin

The Adelaide Superbasin (Lloyd et al., 2020) is a large, Neoproterozoic to middle Cambrian sedimentary system that comprises the Adelaide Rift Complex, contiguous with the Stuart Shelf and Coomalarnie Platform, and the Cambrian Arrowie and Stansbury basins (Figure 3). It is situated at the southeast margin of Proterozoic Australia and formed as a result of the breakup of the Rodinia supercontinent (Figure 1). The depositional history of the Adelaide Superbasin spans over 300 million years, with present day outcrop extending from the Flinders Ranges in South Australia, south onto Kangaroo Island, and east into New South Wales and Victoria. The superbasin began as an intracontinental rift system that successfully progressed to a passive margin in its southeast region yet remained a failed rift in the north (Lloyd et al., 2022; Powell et al., 1994; Preiss, 2000). Deposition within the basin ceased during the Delamerian orogeny c. 514–490

Ma (Drexel and Preiss, 1995; Foden et al., 2006, 2020; Preiss, 2000). Formal lithostratigraphy of the Adelaide Superbasin is divided into three supergroups (Preiss, 2000), two for the Neoproterozoic sequences and a third for the Cambrian sequences, with numerous group and subgroup level divisions (Figure 4). In the Neoproterozoic, the Warrina Supergroup includes the Callanna, Burra, and Poolamacca groups, and the Heysen Supergroup contains the Umberatana, Wilpena, Torrowangee, and Farnell groups. Each of these groups are further divided into numerous subgroups. The reader is referred to Preiss (1987, 2000), Counts (2017), Lloyd et al. (2020, 2022), and references therein for further detail on the geological history of the Adelaide Superbasin.

2.2 Burra Group

The Burra Group is the first widely preserved and exposed series of rocks in the Adelaide Rift Complex of the Adelaide Superbasin. The group contains a generally thick sequence of siliciclastic and carbonate rocks (Figure 5) and is divided into four subgroups (Preiss, 1987, 2000; Preiss and Cowley, 1999). It unconformably overlies the Callanna Group near the margins of the basin but the true stratigraphic relationship between the two groups in areas of a more complete sequence of Callanna Group is not known (Preiss, 1987). Circumstantial evidence has been used to infer a regional unconformity (e.g. Murrell, 1977). The Burra Group unconformably overlies basement in the southern area of the basin (South Mount Lofty Ranges). In turn, it is unconformably overlain by the Umberatana Group, with the termination of the Burra Group occurring at the boundary between the Tonian and Cryogenian periods, marking the start of the Sturtian Glaciation in South Australia.

The basal Emeroo Subgroup is the oldest subdivision and is made of primarily arenaceous rocks with minor dolomitic rocks and mafic volcanic rocks (Figure 5). The base of the Burra Group is defined as the first influx of coarse clastic material after the Curdimurka Subgroup of the Callanna Group (Preiss, 1993). In the south of the basin, the Emeroo Subgroup remains as coarse clastic rocks, but in all other areas it transitions to finer clastic and carbonate sequences before transitioning back to coarser clastic rocks. The top of the Emeroo Subgroup is marked by a widespread series of laterally correlative quartzites/sandstones (e.g. Copley Quartzite, Wortupa Quartzite) that conformably transition into the primarily dolomitic sequences of the Mundallio Subgroup (e.g. the Skillogee Dolomite, the Montacute Dolomite). Minor c. 790 Ma volcanism is known to occur within the Skillogee Dolomite and is believed to be responsible for mineralisation (Preiss et al., 2009) at the historic Burra Copper Mine, which produced ~2.7 million tonnes of copper ore during its lifetime (Drexel, 2008). A significant amount of variation is present within the lithologies of the Skillogee

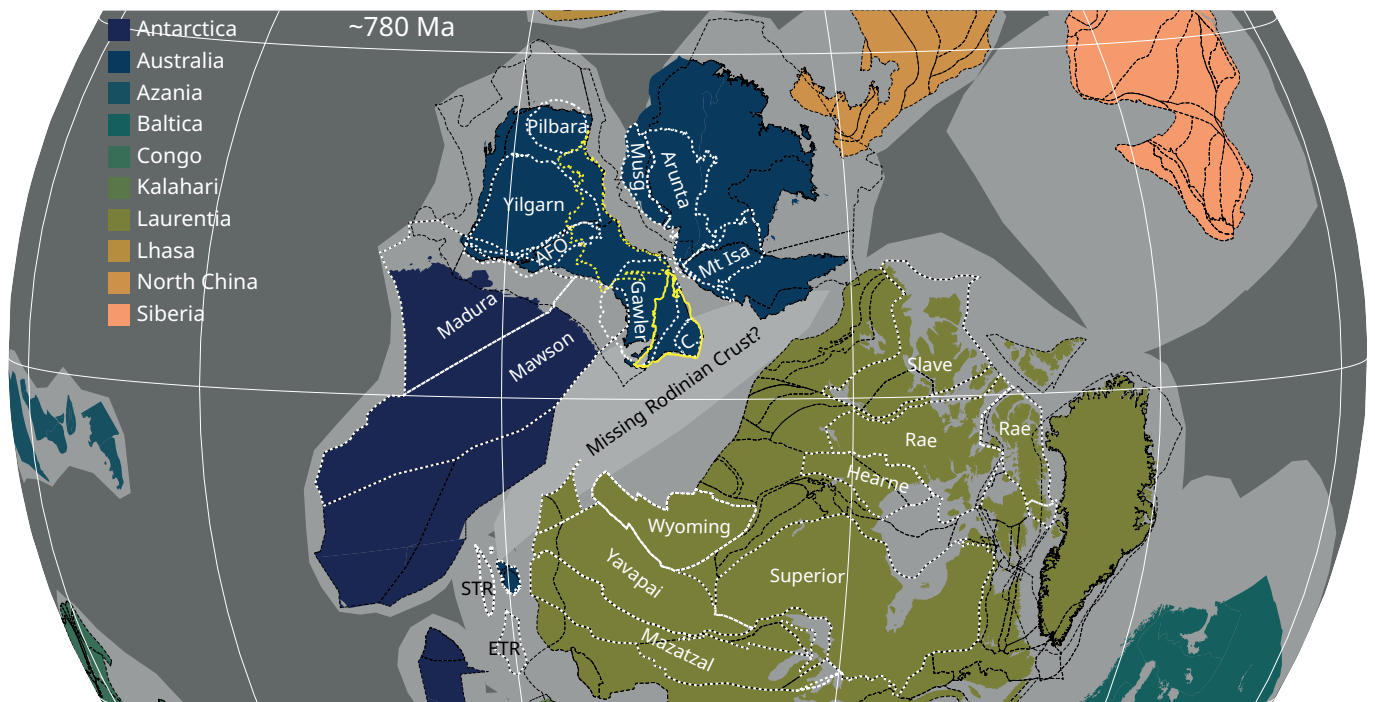


Figure 1 – Plate tectonic reconstruction of north-western Rodinia at c. 780 Ma. Mid-grey shaded polygons represent approximate, predicted overall continental areas at time of reconstruction. Coloured polygons show present-day exposed continental areas and coastlines. Dashed black lines are the present-day terrane boundaries. Dashed white lines highlight some of the key terranes either directly mentioned, or relevant to this research (not all potential detritus sources are highlighted due to overplotting, e.g. north-west Laurentia). Dashed yellow line is present-day extent of the Officer Basin, and the solid yellow line is the present-day extent of the Neoproterozoic portion of the Adelaide Superbasin. ABBREVIATIONS: AFO = Albany Fraser Orogen; C. = Curnamona Province; Musg. = Musgrave Province; ETR = East Tasman Rise; STR = South Tasman Rise. 3D orthographic projection generated in GPLates (Mulder *et al.*, 2018a) using the model of Cao *et al.* (2024).

Dolomite and its equivalents, but sedimentary magnesite and abundant dolostones characterise this subgroup (Counts, 2017; Preiss, 1987, 2000; Uppil, 1980; Virgo *et al.*, 2021, 2023). Geochronology supports correlation of the Boucaut Volcanics to the volcanics occurring within the Skillogalee Dolomite c. 790 Ma (Armistead *et al.*, 2020; Preiss *et al.*, 2009).

After deposition of the mostly paralic sedimentary sequences of the Mundallio Subgroup, the conformably overlying Bungarider Subgroup sees a return to increasingly clastic deposition (Counts, 2017; Preiss, 2000; Virgo *et al.*, 2021, 2023), with subsequent sourceward-shifting to basinward-shifting facies tracts (Figure 5). The Belair Subgroup is only present in the south and east of the basin. It is incompletely understood but shows greater lithological similarity to the underlying Bungarider Subgroup than it does to the overlying Umberatana Group (Counts, 2017). At its base, the Belair Subgroup consists of coarse-grained quartzites, with an overall sourceward-shifting facies tract to the upper, predominantly shale sequences (Figure 5). Very rare limestones in the uppermost Mintaro Shale allow for the possibility of minor shore ice (Preiss, 2000).

2.3 Umberatana Group

The Umberatana Group disconformably overlies the Burra Group, and is further divided into the Yudnamutana, Nepouie, and Yerelina subgroups.

The Yudnamutana Subgroup is made up of glaciogenic rocks attributed to the Sturtian Glaciation, dominated by globally significant, characteristic diamictites of the Sturt Formation (Lloyd *et al.*, 2023). The overlying Nepouie subgroup marks the first basin-wide flooding event, signified by the ubiquitous Tapley Hill Formation (Preiss, 1987, 1993, 2000). Further detail on the stratigraphy of Yudnamutana and Nepouie Subgroups is found in Preiss (1987, 2000), Preiss *et al.* (1998), and Lloyd *et al.* (2023). The Yerelina Subgroup overlies the Nepouie Subgroup and is detailed further here.

2.3.1 Yerelina Subgroup

The Yerelina Subgroup is the uppermost division of the Umberatana Group and represents the Marinoan (Elatina) Glaciation in South Australia. The equivalent subgroup in New South Wales is thought to be the Teamsters Creek Subgroup (Cooper and Tuckwell, 1971; Fitzherbert and Downes, 2015; Preiss, 1987; Sheibner and Basden, 1998). In the far northeast (North Flinders Ranges) and southeast to east of the basin (North Mount Lofty Ranges, Nackara Arc), the Fortress Hill Formation is the lowermost formation in the subgroup and represents the onset of glacial conditions, marked by the presence of small dropstones and limestones, and occasional boulders within laminated siltstones (Lindsay, 1973; Preiss *et al.*, 1998). The abundance of clasts increases toward the top of the formation, and the

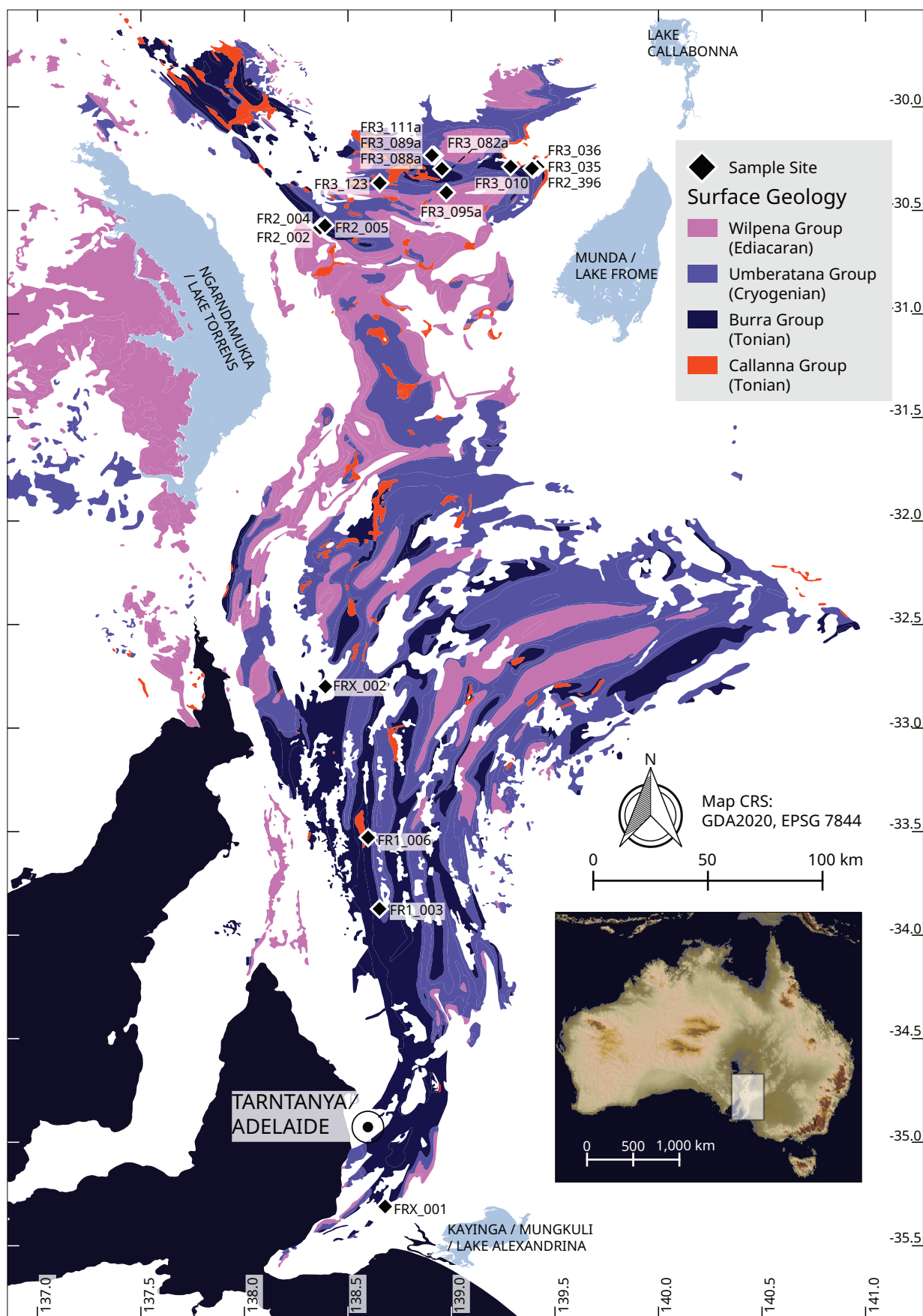


Figure 2 – Map showing surface geology distribution of the Neoproterozoic sequences of the Adelaide Rift Complex, Stuart Shelf, and Coomalbarnie Platform. Sample sites from this study are indicated by diamonds. For GPS coordinates of the sample sites see data availability. Inset map shows location of main map relative to the Australian landmass as a colour shade map overlain on hill shaded GMTED2010 7.5s digital elevation model, publicly available from the United States Geological Survey (*Danielson and Gesch, 2011*).

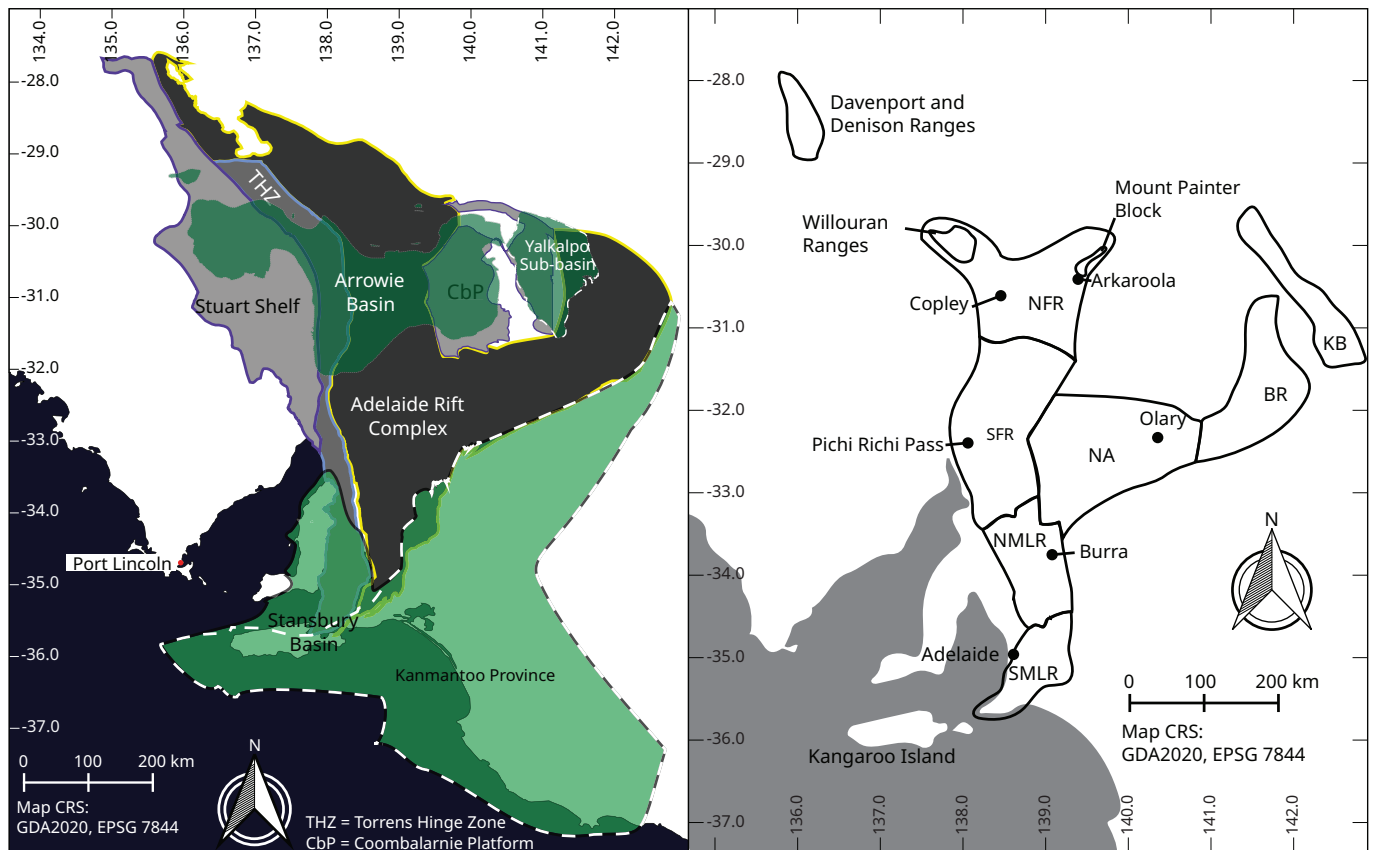


Figure 3 – Left: Subdivisions of the Adelaide Superbasin. Greys are the Neoproterozoic basins; greens are the Cambrian basins. Right: Geographic divisions of the Adelaide Superbasin referred to in text. Abbreviations: MLR-Mount Lofty Ranges, FR-Flinders Ranges (N=North, S=South); NA-Nackara Arc; BR-Barrier Ranges; KB-Koonenberry Belt.

presence of crossbedding and sinuous ripple marks are suggested to indicate overall shallowing of the formation (Lindsay, 1973).

The Mount Curtis Tillite and Gumbowie Arkose overlie the Fortress Hill Formation. Along with the Pepuarta Tillite (which conformably overlies the Gumbowie Arkose), the Mount Curtis Tillite is believed to represent the peak glacial conditions during this time. These units were interpreted to be deposited under high-energy, shallow-water conditions (Preiss *et al.*, 1998) with clear glacial origin indicated by faceted and striated boulders within the diamictites (Williams *et al.*, 2008). These in turn are overlain by the deglacial Balparana Sandstone, Grampus Quartzite, and Ketchowla Siltstone. In the far south (Adelaide area), central (South and North Flinders Ranges) and west (Stuart Shelf) of the basin (Figure 3), the Elatina Formation and Whyalla Sandstone are the correlatives of the aforementioned units, except for the Fortress Hill Formation.

The Elatina Formation is much thinner than its putative equivalents further north. At its maximum it reaches up to 300 m thickness (Rose *et al.*, 2013), compared to the correlative Mount Curtis Tillite and Balparana Sandstone that get up to ~1000 m thick (Preiss, 1993). The Elatina Formation contains significant variation in lithology from glaciofluvial to deltaic and shallow marine sandstones, glaciomarine

diamictites, siltstones and mudstones with ice-rafted drop stones, and tidal rhythmites (Le Heron *et al.*, 2011; Le Heron, 2012; Preiss, 1993, 2000; Rose *et al.*, 2013; Williams *et al.*, 2008). The Whyalla Sandstone as currently defined contains a characteristic peri-glacial aeolian sandstone (Williams *et al.*, 2008; Williams and Tonkin, 1985) with fluvial to deltaic and marine variations (McAvaney *et al.*, 2016; Tonkin and Wallace, 2021). The Yerelina Subgroup is overlain by a distinct cap carbonate in almost all areas, marking the end of the Marinoan (Elatina) Glaciation. This cap carbonate is globally ubiquitous and dated at c. 635 Ma (Calver *et al.*, 2013; Rooney *et al.*, 2015).

2.4 Wilpena Group

The Wilpena Group is the uppermost Neoproterozoic division in the Adelaide Superbasin and is broadly divided into two upward shoaling sequences. The lowest of these corresponds to the Sandison Subgroup. This subgroup begins with the Nuccaleena Formation (the cap carbonate of the Marinoan Glaciation), which is generally overlain by, but partially coeval to the Seacliff Sandstone. These units are in turn overlain by the Brachina Formation and its equivalents, predominantly shales and siltstones that shallow upward into the ABC Range Quartzite (Counts, 2017; Preiss, 1987, 2000).

The second upward shoaling sequence overlies the Sandison Subgroup. As currently defined, it begins

ICS	SG	G	Subgroup	South Mount Lofty Ranges	North Mount Lofty Ranges	Nackara Arc	South Flinders Ranges	North Flinders Ranges (Willouran Ranges)	North Flinders Ranges	NE North Flinders Ranges			
Ediacaran	538.8 Ma	Wilipena	Pound				Rawnsley Quartzite (570 ± 23 Ma)		Rawnsley Quartzite (570 ± 23 Ma)	Billy Springs Formation (564 ± 25 Ma)			
			Depot Springs				Bonney Sandstone (579 ± 32 Ma)		Bonney Sandstone (611 ± 20 Ma)				
			Aruhna										
			Sandision				ABC Range Quartzite (630 ± 16 Ma)		Brachina Formation (609 ± 64 Ma Rb-Sr)				
		Heysen	c. 635 Ma	Yeralina	Elatina Formation (671 ± 52 Ma)						Elatina Formation (671 ± 52 Ma)	Balparana Sandstone (946 ± 31)	
											Mount Curtis Tillite (1032 ± 36 Ma)	Fortress Hill Formation (977 ± 36 Ma)	
				Upalinna				Yaltipena Formation (662 ± 20 Ma)			Trezona Formation (674 ± 11 Ma)		
					Wilmington Formation (688 ± 8 Ma)					Amberoo Formation (1110 ± 71 Ma)			
				Nepouie						Tapley Hill Formation (654 ± 13 Ma)			
										Tindelpina Shale Member (645.1 ± 4.8 Ma Re-Os)			Serle Conglomerate (1291 ± 50 Ma)
Yudhamutana				Wilyerpa Formation (1502 ± 70 Ma)				Tuff in Wilyerpa (663 ± 0.76 Ma)	Lyndhurst Formation (1174 ± 19 Ma)				
	Sturt Formation (714 ± 28 Ma)	Sturt Formation (1774 ± 39 Ma)	Sturt Formation	Sturt Formation (667 ± 6 Ma)	Sturt Formation (673 ± 19 Ma)	Sturt Formation (666 ± 25 Ma)			Sturt Formation (891 ± 15 Ma)				
									Fitton Formation (1162 ± 49 Ma)				
Tonian	c. 720 Ma	Burra	Belair	Mitcham Quartzite (734 ± 42 Ma)	Gilbert Range Quartzite (731 ± 34 Ma)								
			Bungarider	Stonyfell Quartzite (1592 ± 36 Ma)			Saddleworth Formation (956 ± 16 Ma)			Myrtle Springs Formation (810 ± 42 Ma)			
			Mundallio			Skillogalee Dolomite (789 ± 9 Ma)		Skillogalee Dolomite (857 ± 16 Ma)		Skillogalee Dolomite (925 ± 13 Ma)			
		Emeroo				Koorunga Member porphyry (794 ± 4)							
						Boucaut Volcanics (788 ± 6 Ma)		Copley Quartzite (1129 ± 51 Ma)	Copley Quartzite (838 ± 15 Ma)	Wortupa Quartzite (857 ± 18 Ma)			
			Rhynie Sandstone (1513 ± 26 Ma)					Top Mount Sandstone (841 ± 21 Ma)		Opaminda Formation (1374 ± 21 Ma)			
		Callanna					Oodla Wirra Volcanics (798 ± 5 Ma, 799 ± 4 Ma)				Blue Mine Conglomerate (1081 ± 19 Ma)		
											Humanity Seat Formation (1053 ± 114 Ma)		
			Curdimurka		Niggly Gap Beds (1571 ± 12 Ma)				Rook Tuff (802 ± 10 Ma)				
									Dome Sandstone (993 ± 62 Ma)				
			Mount Crawford Granite Gneiss (812 ± 6 Ma)										
Arkaroola									Wooltana Volcanics (830 ± 50 Ma)				
									Paralana Quartzite (893 ± 9 Ma)				

Figure 4 – Stratigraphic table showing supergroup (SG), group (G), and subgroup divisions of the Neoproterozoic successions of the Adelaide Superbasin. Formations with available geochronology are shown according to their geographic locality (headers). Yellow shading indicates formations with MDAs new from this study, or where new data has been added to existing data from *Keeman et al. (2020)* and *Lloyd et al. (2020)*, mauve shading indicates data from *Lloyd et al. (2023)*, white shading indicates detrital data from *Keeman et al. (2020)* and *Lloyd et al. (2020)*, and purple shading indicates non-detrital chronology. Adapted from *Lloyd et al. (2020)*.

with the Aruhna Subgroup (Bunyerroo Formation and equivalent Yarloo Shale) and is then overlain by the Depot Springs Subgroup (Wonoka Formation, Wearing Dolomite). However, the separation into the Aruhna and Depot Springs subgroups

remains conjectural and are likely unwarranted (*Preiss, 2000*). The Bunyerroo Formation and Yarloo Shale are thought to have been deposited under a cold-water, generally deep-marine setting in an overall transgressive sequence (*Young, 1995*).

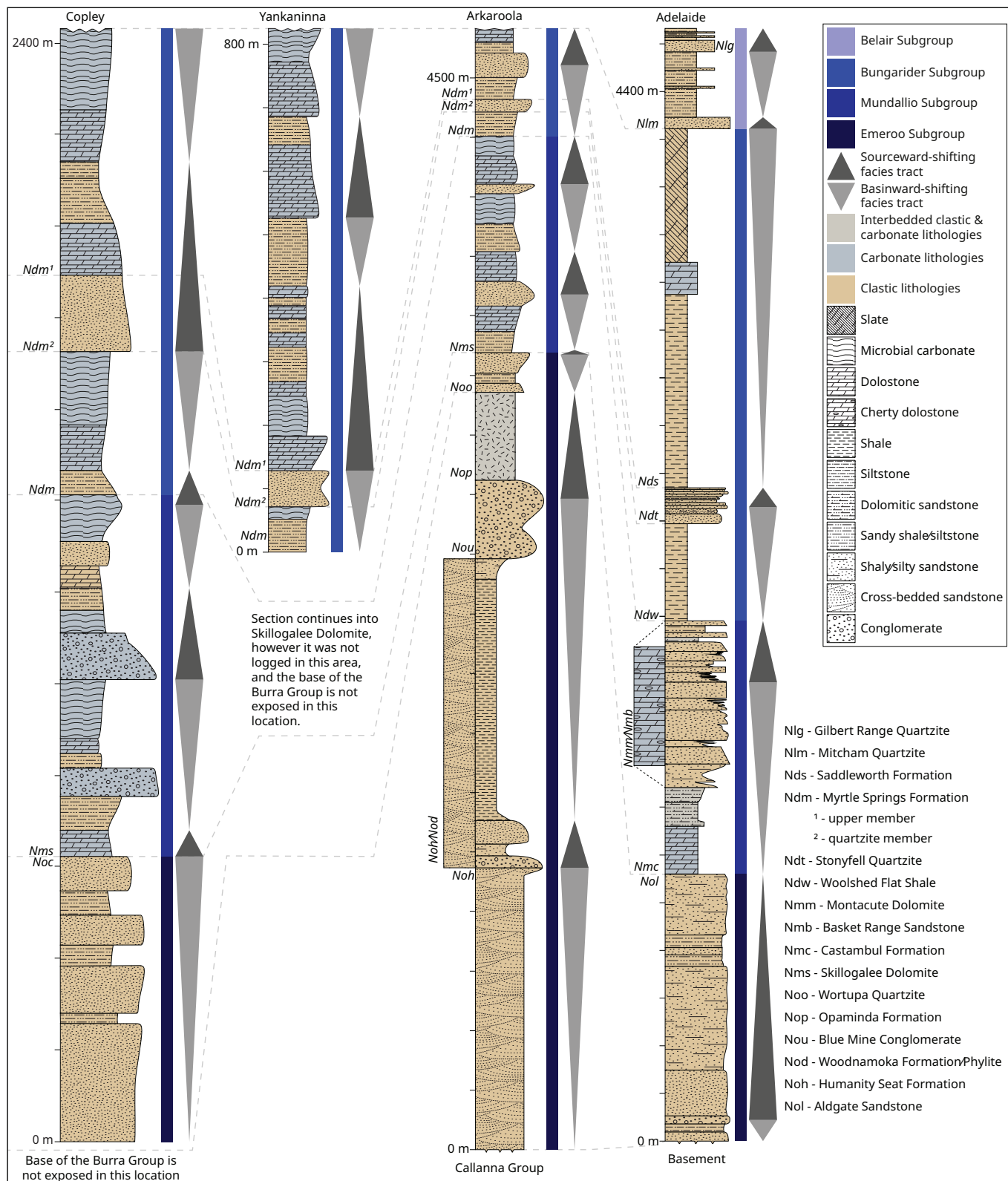


Figure 5 – Generalised stratigraphic columns with correlation lines of the Burra Group from the south and north of the basin with corresponding, high level, tectonic sequence stratigraphy facies. Tectonic successions follow terminology of *Matenco and Haq (2020)*, sourceward-shifting facies tracts are where accommodation space is created faster than the rate of sediment supply ($\delta AS/SS \geq 1$) and basinward-shifting facies tracts are where the rate of sediment supply outdoes the creation of accommodation space ($\delta AS/SS \leq 1$). Stratigraphic logs compiled from *Preiss (1987, 1997)*, *Preiss and Cowley (1999)*, *Uppil (1980)*, and *Virgo et al. (2021, 2023)*. For location references, refer to the map figures.

Notably, the Bunyeroo Formation and Yarloo Shale contain a distinct layer interpreted as a bolide impact debris layer related to an impact site at Lake Acraman (*Gostin et al., 1986, 1989*). The Wonoka Formation has

been subject to numerous studies (e.g. *Eickhoff et al., 1988*; *Giddings et al., 2010*; *Haines, 1987*; *Retallack et al., 2014*; *Urlwin, 1992*) owing to the presence of deeply incised canyons and a strongly negative $\delta^{13}C$

anomaly known as the Shuram-Wonoka excursion (*Williams and Schmidt, 2018*).

The overlying Pound Subgroup is the uppermost division of the Wilpena Group, and the last of the Neoproterozoic sequences in the Adelaide Superbasin. It contains three formations, the basal Bonney Sandstone and the overlying Rawnsley Quartzite (*Counts, 2017*). Both formations are replaced by the Billy Springs Formation in the far northeast Flinders Ranges (*Counts and Amos, 2016; Sheard, 2012*). The Bonney Sandstone primarily consists of fine to medium grained, reddish quartz arenites to feldspathic sandstones but is occasionally coarse-grained. It is interpreted to have been deposited in a tidally influenced marginal marine environment, with some support for a tidal-estuary system (*Gehling, 1982; Preiss, 1987*). However, a more recent study in the type area did not determine conclusive evidence for tidal influence, instead suggesting a fluvially dominated deltaic sequence, with only a small contribution from waves and tides (*Counts et al., 2016*). Both studies concur that Bonney Sandstone is a shallowing upward sequence. One formal member is defined for the Bonney Sandstone, the carbonate rich Patsy Hill Member (*Preiss and Cowley, 1999*). The Bonney Sandstone disconformably underlies the Chace Quartzite Member of the Rawnsley Quartzite, whilst locally also being incised by the Ediacara Member (*Gehling and Droser, 2012*). Overall, the Rawnsley Quartzite is made up of cleaner sandstones than those of the Bonney Sandstone and is thought to be deposited as a shallow marine, wave and tide reworked deltaic succession (*Gehling, 2000; Gehling and Droser, 2012*). The Rawnsley Quartzite is most famous for the Ediacara Member that preserves fossil casts of the Ediacaran fauna (*Gehling and Droser, 2012*), Earth's first confirmed animals (*Bobrovskiy et al., 2018*).

3 Methods

Rock samples were prepared for U–Pb DZ analysis by crushing, sieving, panning and, where necessary due to low zircon yield, heavy liquid separation. Any grain that remotely resembled a zircon was picked to minimise human bias, an issue highlighted by *Sláma and Košler (2012)* and *Dröllner et al. (2021)*. Where permitted by zircon yields, at least 300 zircons were picked per sample, otherwise all zircons in the sample were picked. Cathodoluminescence images were obtained on either a FEI Quanta 600 scanning electron microscope (for zircon analysed in 2020) or a Cameca SXFive Electron Microprobe (for zircon analysed in 2021). The zircons were analysed using Laser Ablation Inductively Coupled Plasma Mass Spectrometry (LA-ICP-MS) to obtain a suite of elemental data for U–Pb geochronology and rare earth element (REE) analysis. All zircons were analysed using a RESOLUTION-LR 193 nm ArF excimer laser ablation system coupled with an Agilent 7900x inductively coupled plasma mass spectrometer. All

analytical instruments used are housed at Adelaide Microscopy, University of Adelaide, Australia.

GJ-1 (*Horstwood et al., 2016; Jackson et al., 2004*) was used as the primary calibration standard for U–Pb ratios, and NIST610 (*Jochum et al., 2011*) was used as the primary calibration standard for Pb isotope ratios and trace element data. The internal standard for trace element data was ^{91}Zr with a value of 431,400 ppm (43.14 wt%) assigned to unknowns. Plešovice (*Horstwood et al., 2016; Sláma et al., 2008*) and 91500 (*Horstwood et al., 2016; Wiedenbeck et al., 1995, 2004*) were used as validation standards. Unknowns were bracketed by two analyses of GJ-1, followed by a combined two to three analyses of Plešovice and 91500, and two analyses of NIST610 every 20–30 unknowns. A 30 second gas blank followed by either a 40 second or 30 second ablation (session on 2021-03-30) time was used with a laser repetition rate of 5 Hz. A spot size of 29 μm and a nominal fluence of 2 $\text{J}\cdot\text{cm}^{-2}$ was used for zircon, and a spot size of 43 μm using a nominal fluence of 3.5 $\text{J}\cdot\text{cm}^{-2}$ was used for NIST610. Data were processed using LADR (*Norris and Danyushevsky, 2018*) version 1.1.06 and output as "Full Analytical Uncertainty". No common Pb corrections were applied to the data. Reference material ratios used for GJ-1, Plešovice, and 91500 were the Chemical Abrasion Isotope Dilution Thermal Ionisation Mass Spectrometry (CA-ID-TIMS) values (uncorrected for thorium disequilibria and common-Pb) of *Horstwood et al. (2016)*. Weighted averages and dispersion statistics for all standards are available from the link in data availability.

Statistical analysis of the zircon U–Pb data follows the method of *Lloyd et al. (2020)*. Data are considered concordant if within $\pm 10\%$, and a "meaningful" age if the uncertainty is $\leq 10\%$ - if a datum satisfies both parameters it is termed a "Filtered Age". Maximum depositional ages (MDAs) are determined from a stricter 2% concordance for a conservative estimate of the youngest single concordant grain. All age uncertainties are quoted at 2-standard error (SE) level. Kernel density estimates (KDEs), and multidimensional scaling plots (MDS) were generated using IsoplotR (*Vermeesch, 2018*). Key zircon trace element data are presented graphically using methods following (*Verdel et al., 2021*) and additionally lanthanoid data are represented using violin plots and lambda representation (*Anenburg and Williams, 2022; O'Neill, 2016*).

Metadata for the LA-ICP-MS sessions, data for all analyses, cathodoluminescence images, and R code used to generate plots are available from the links in 'data and code availability'.

4 Results

Fifteen samples from the Burra Group (FR1_003_01, FR1_006_03, FR2_002_01, FR2_004_01, FR2_005_01, FR2_396, FR3_010, FR3_035, FR3_036, FR3_082a,

FR3_123, FRX_001, FRX_002, ML_008, & SF1), three samples from the Umberatana Group (FR3_088a, FR3_089a, & FR3_111a), and three samples from the Wilpena Group (058, 319, & FR3_095a) were analysed for U–Pb DZ data (Figure 4). Several samples had naturally low zircon yields (FR1_006_03, FR3_035, FR3_036, FR3_088a, FR3_089a, FR3_111a, & FRX_001). Additional zircon analyses on samples 058 and 319 from *Lloyd et al.* (2020) were run during this study. The methodology used for provenance assessment has resulted in unreliably young ‘ages’ for the youngest grains in the Minburra Quartzite Member and Billy Springs Formation. This is attributed to be an artefact of concordance determination outlined in the methods section, and mostly likely a result of minor Pb-loss post crystallisation. This highlights the need to use a conservative and strict method for determining MDAs when using youngest single grains. As is outlined in the method section, we have used a stricter 2% concordance filter to determine sample MDAs.

4.1 Burra Group

A total of 28 zircons were analysed from sample FR3_036 (Humanity Seat Formation) with 26 passing filtering parameters. Grain ages range from 2535 ± 32 Ma to 1017 ± 18 Ma, with a primary population peak c. 1640 Ma, and a secondary population peak c. 2480 Ma (Figure 6).

A total of 40 zircons were analysed from sample FR3_035 (Blue Mine Conglomerate) with 38 passing filtering parameters. Grain ages range from 2978 ± 32 Ma to 1079 ± 17 Ma, with a primary population peak c. 1710 Ma, and a secondary population peak c. 2480 Ma (Figure 6).

A total of 89 zircons were analysed from sample FR2_396 (Opaminda Formation) with 66 passing filtering parameters. Grain ages range from 3164 ± 32 Ma to 1117 ± 17 Ma, with a primary population peak c. 1590 Ma. Subordinate population peaks are present c. 3130 Ma, c. 2640 Ma, c. 2480 Ma, c. 1760 Ma and c. 1410 Ma (Figure 6).

A total of 56 zircons were analysed from sample FR3_010 (Wortupa Quartzite) with 56 passing filtering parameters. Grain ages range from 3239 ± 59 Ma to 845 ± 13 Ma, with a primary population peak c. 1720–1640 Ma, and a subordinate population peaks c. 3120 Ma, c. 2400 Ma, and c. 1000 Ma (Figure 6).

A total of 122 zircons were analysed from sample FR3_123 (Copley Quartzite, Yankaninna area), with 118 passing filtering parameters. Grain ages range from 3152 ± 27 Ma to 864 ± 16 Ma with a primary population peak c. 1720 Ma, and a subordinate population peaks c. 2430 Ma, and c. 1620 Ma (Figure 6).

A total of 117 zircons were analysed from sample FR2_002_01 (Copley Quartzite, Copley area, base), with 112 passing filtering parameters. Grain ages range from 3254 ± 36 Ma to 1195 ± 20 Ma, with a

primary population peak c. 1750 Ma. Subordinate population peaks are present at c. 3050 Ma, c. 2720 Ma, and c. 2480 Ma (Figure 6).

A total of 120 zircons were analysed from sample FR2_004_01 (Copley Quartzite, Copley area, top), with 117 passing filtering parameters. Grain ages range from 3252 ± 33 Ma to 838 ± 13 Ma, with a primary population peak c. 1130 Ma. Subordinate population peaks are present c. 2490 Ma, and c. 1690 Ma (Figure 6).

A total of 198 zircons were analysed from sample FR3_082a (Myrtle Springs Formation), with 176 passing filtering parameters. Grain ages range from 3451 ± 36 Ma to 807 ± 16 Ma, with a primary population peak c. 1000 Ma. Subordinate population peaks are present c. 2490 Ma, c. 1800 Ma, and c. 1280 Ma (Figure 6).

A total of 171 zircons were analysed from sample SF1 (Stonyfell Quartzite), with 164 passing filtering parameters. Grain ages range from 3122 ± 35 Ma to 1536 ± 28 Ma, with a prominent primary population peak c. 1840 Ma. Minor population peaks are present at c. 2500 Ma, c. 2000 Ma, c. 1740 Ma, and c. 1590 Ma (Figure 6).

A total of 143 zircons were analysed from sample FRX_002 (Saddleworth Formation, Minburra Quartzite Member), with 83 passing filtering parameters. Grain ages range from 2556 ± 40 Ma to 692 ± 15 Ma, with a primary population peak c. 1130 Ma. Subordinate population peaks are present c. 2470 Ma, and c. 1540 Ma (Figure 6).

Sample FR1_006_03 (Saddleworth Formation), had low zircon yield. In total only 11 zircons were analysed with 9 passing filtering parameters. Grain ages range from 2815 ± 38 Ma to 1562 ± 27 Ma. Due to the limited number of analyses and significant spread in ages, the KDE forms a broad spectrum (Figure 6).

Sample FRX_001 (this sample was collected from a formation that has previously been mapped as a correlative of the Gilbert Range Quartzite), had low zircon yield. Only 23 zircons were analysed with 17 passing filtering parameters. Grain ages range from 1682 ± 31 Ma to 988 ± 17 Ma, forming a predominant population peak at c. 1160 Ma (Figure 6).

A total of 113 zircons were analysed from sample ML_008 (Mitcham Quartzite) with 93 passing filtering parameters. Grain ages range from 3746 ± 41 Ma to 726 ± 13 Ma, with a primary population peak c. 1080 Ma. Subordinate population peaks are present c. 1630 Ma, c. 1400 Ma, c. 930 Ma, and c. 740 Ma (Figure 6).

4.2 Umberatana Group

Sample FR3_111a (Fortress Hill Formation), had low zircon yield. This sample was collected from a very fine sandy lithology within a formation of mostly siltstone. A total of 19 zircons were analysed with 18

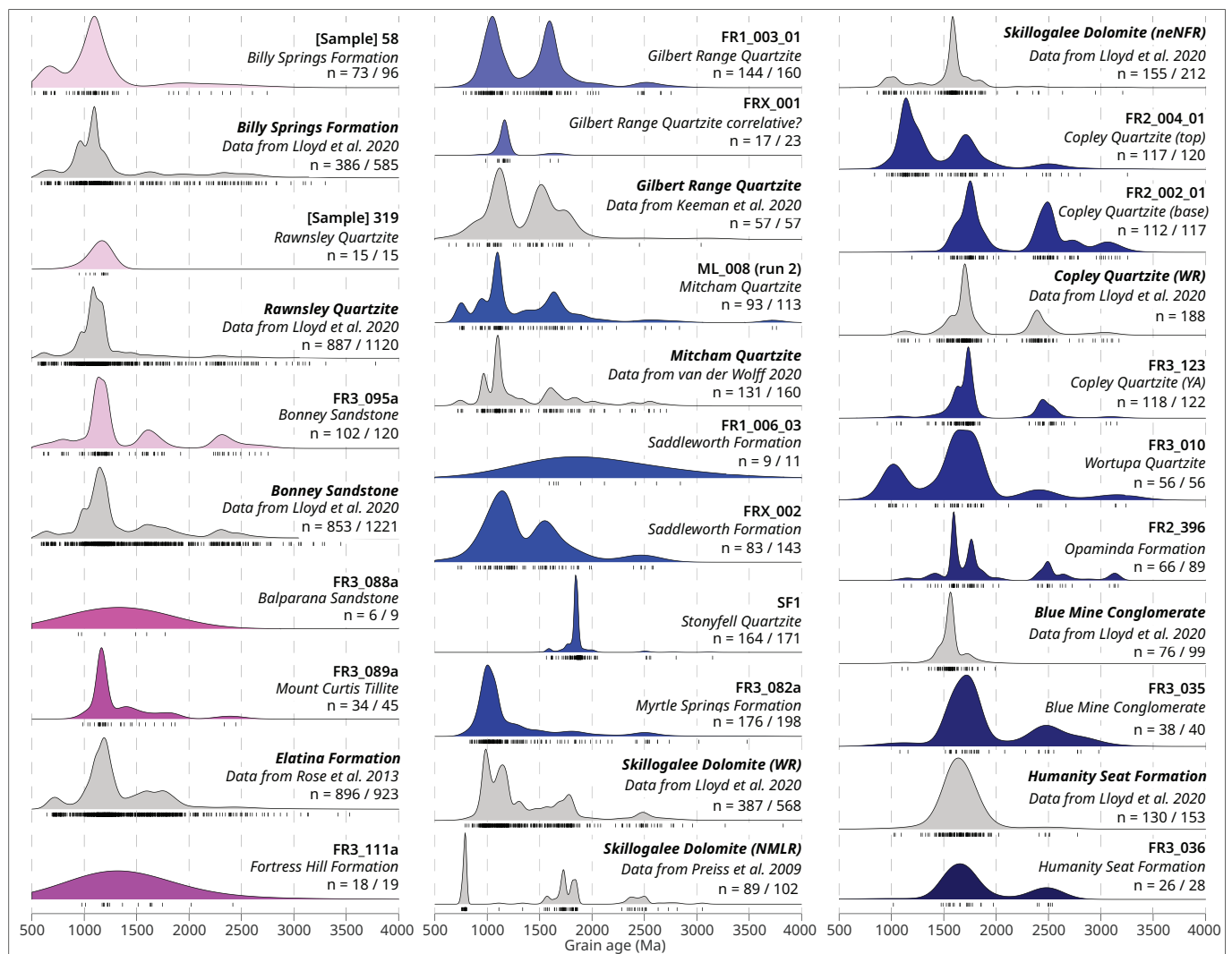


Figure 6 – Kernel density estimates [KDEs] of detrital zircon populations from each sample. Coloured KDEs are from data collect in this study, while grey KDEs are from published sources as denoted. Tick marks below each plot represent an analysis. n = filtered analyses / total analyses. Generated using IsoplotR (Vermeesch, 2018). Abbreviations: WR = Willouran Ranges; neNFR = north-eastern North Flinders Ranges; YA = Yankaninna area/anticline; NMLR = North Mount Lofty Ranges

passing filtering parameters. Grain ages range from 2417 ± 67 Ma to 976 ± 15 Ma. Due to the limited number of analyses and significant spread in ages, the KDE forms a broad spectrum (Figure 6).

Sample FR3_089a (Mount Curtis Tillite), had low zircon yield. A total of 45 zircons were analysed over two analytical sessions, with 34 passing filtering parameters. Grain ages range from 2444 ± 25 Ma to 986 ± 18 Ma, with a predominant population peak c. 1160 Ma (Figure 6).

Sample FR3_088a (Balparana Sandstone), had extremely low zircon yield. A total of 9 zircons were analysed over two analytical sessions, with only 6 passing filtering parameters. Grain ages range from 1771 ± 24 to 944 ± 14 Ma. Due to the extremely limited number of analyses and significant spread in ages, the KDE forms a broad spectrum (Figure 6).

4.3 Wilpena Group

A total of 120 zircons were analysed for sample FR3_095a (Bonney Sandstone), with 102 passing

filtering parameters. Grain ages range from 2752 ± 48 Ma to 610 ± 9 Ma, with a primary population peak c. 1120 Ma. Subordinate population peaks are present c. 2310 Ma, c. 1590 Ma, and c. 790 Ma (Figure 6).

An additional 15 zircons from sample 319 (Lloyd *et al.*, 2020, Rawnsley Quartzite), were analysed during this study to gain some geochemical data for the zircons in this sample. All 15 passed filtering parameters with grain ages range from 1215 ± 14 to 949 ± 15 Ma. Due to the extremely limited number of analyses the KDE forms a broad spectrum with a central peak c. 1160 Ma (Figure 6).

An additional 96 zircons from sample 058 (Lloyd *et al.*, 2020, Billy Springs Formation), were analysed during this study to gain some geochemical data for the zircons in this sample. A total of 73 analyses passed filtering parameters, with grain ages ranging from 2743 ± 40 Ma to 527 ± 8 Ma. A primary population peak is present c. 1580 Ma, with a secondary population peak c. 660 Ma (Figure 6).

4.4 Zircon Trace Element Geochemistry

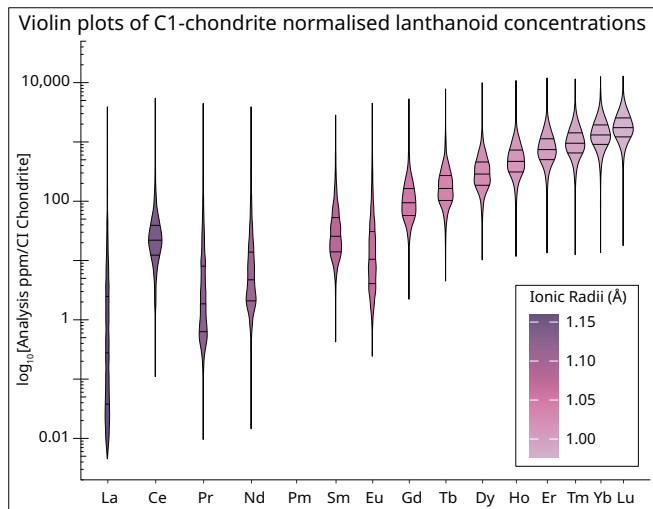


Figure 7 – Violin plots of C1 chondrite (O'Neill, 2016) normalised lanthanoids for all filtered zircon analysed in this study. X-axis is spaced by ionic radii (Shannon, 1976) and ordered by atomic number. Black lines across the fill of each plot represent the 0.25, 0.5, and 0.75 quantiles. Bandwidth of the density estimates is calculated using the Botev algorithm from the Provenance package (Vermeesch et al., 2016).

Most analyses resolved lanthanoid concentrations that are typical for zircons, with several orders-of-magnitude increase in concentration from light to heavy elements, a slight negative deviation in europium (Eu), and a positive deviation in cerium (Ce) (Figure 7). Two analyses (FR3_095a - 032, and FR3_089a - 034) have lanthanoid concentrations atypical of zircon, with overall positive (based on ionic radii) slopes (λ_1 of +9.03, and +3.72) due to highly elevated light lanthanoids (La to Nd). Overall, the lanthanoid pattern for both analyses have a concave-up shape ($+\lambda_2$) with mid to heavy lanthanoid concentration increasing as would normally occur in zircon. Major element percentages, ~13.25 wt% and ~18.57 wt% silicon, suggest these two analyses are zircon, and CL images also support this. It is likely these two analyses have gone through complicated zones of inclusions not visible on the CL images of the grain surfaces. Another noticeable anomaly is present on Figure 8, where one Ce* c. 1700 Ma is significantly greater than any other analysis. This analysis is FR3_036 - 016 and has a Ce* value of ~230,000. This is anomalous as both La and Pr were below detection limit, and the zircon has a low average lanthanoid concentration (λ_0 of -0.5495). As such, this Ce* value is considered unreliable.

5 Discussion

5.1 Zircon Trace Element Geochemistry

The U/Yb against Y plot (Figure 9) indicates that most zircons analysed in this study were generated in continental crust with a small number of younger zircons potentially of oceanic affinity (Grimes et al.,

2007, 2015). Nearly all zircons have a Th/U >0.07 and are inferred to be originally generated as magmatic rather than metamorphic zircon (Collins et al., 2004; Rubatto, 2002). Lanthanoid concentrations, C1 chondrite normalised (O'Neill, 2016), are generally typical of zircon (Figure 7) with a positive pattern slope (increasingly negative λ_1 values) from light to heavy lanthanoids, a positive Ce anomaly, and negative Eu anomaly (Hoskin and Ireland, 2000; Hoskin, 2003). There are no significant trends in lanthanoid pattern slope or curvature (Figure 8), denoted as λ_1 (linear slope), λ_2 (quadratic slope), and λ_3 (cubic slope) (Anenburg and Williams, 2022), with time or sample. Both Eu and Ce anomalies (denoted by Eu* and Ce*) show a significant spread through time. However, an increasing number of zircons c. 1000 Ma show low (i.e. deep) Eu* anomalies with greater data spread. Additionally, post 1000 Ma zircons show a minor trend towards higher Eu*, and correspondingly lower Ce*, suggesting zircon growth in competition with plagioclase, and not reflective of magma oxidation state (Verdel et al., 2021). These trends are of little use for provenance determinations, however, may be useful as part of a larger study to better understand the regional geologic (magmatic) history.

5.2 Maximum Depositional Ages (MDAs)

MDAs from this study and published literature are presented with a stratigraphic table in Figure 4. Sample locations are shown in Figure 2 with Figure 3 showing regional geographic areas. As highlighted in the results, MDAs quoted here differ from the youngest grain quoted in the results section. A conservative method is employed so that only high confidence (within 2% of concordance) grain age determinations are considered. We quote single grain ages as MDAs (following Spencer et al., 2016) due to the lack of any a priori reason that any two grains in a sediment should be the same age.

5.2.1 Burra Group

Several age constraints for the samples from the Burra Group exist. A limit defining the oldest age possible for Burra Group rocks is 802 ± 10 Ma from the Rook Tuff within the upper Curdimurka Subgroup, although the reliability of this age is questioned (Lloyd et al., 2022). Within the Burra Group an age of 788 ± 6 Ma has been determined for the Boucaut Volcanics (Armistead et al., 2020). While the exact stratigraphic position of the Boucaut Volcanics remains unresolved (Lloyd et al., 2020), it lies within the lower Burra Group, likely at the top of the oldest Emeroo Subgroup. This is based on the similar age (794 ± 4 Ma, Preiss et al., 2009) obtained for a syndepositional volcanic porphyry within the Skillogalee Dolomite of the overlying Mundallio Subgroup. Additionally, an intrusive bimodal volcanic sequence only preserved in diapiric breccia of the underlying Callanna Group, the Oodla Wirra Volcanics, has two prior age determinations

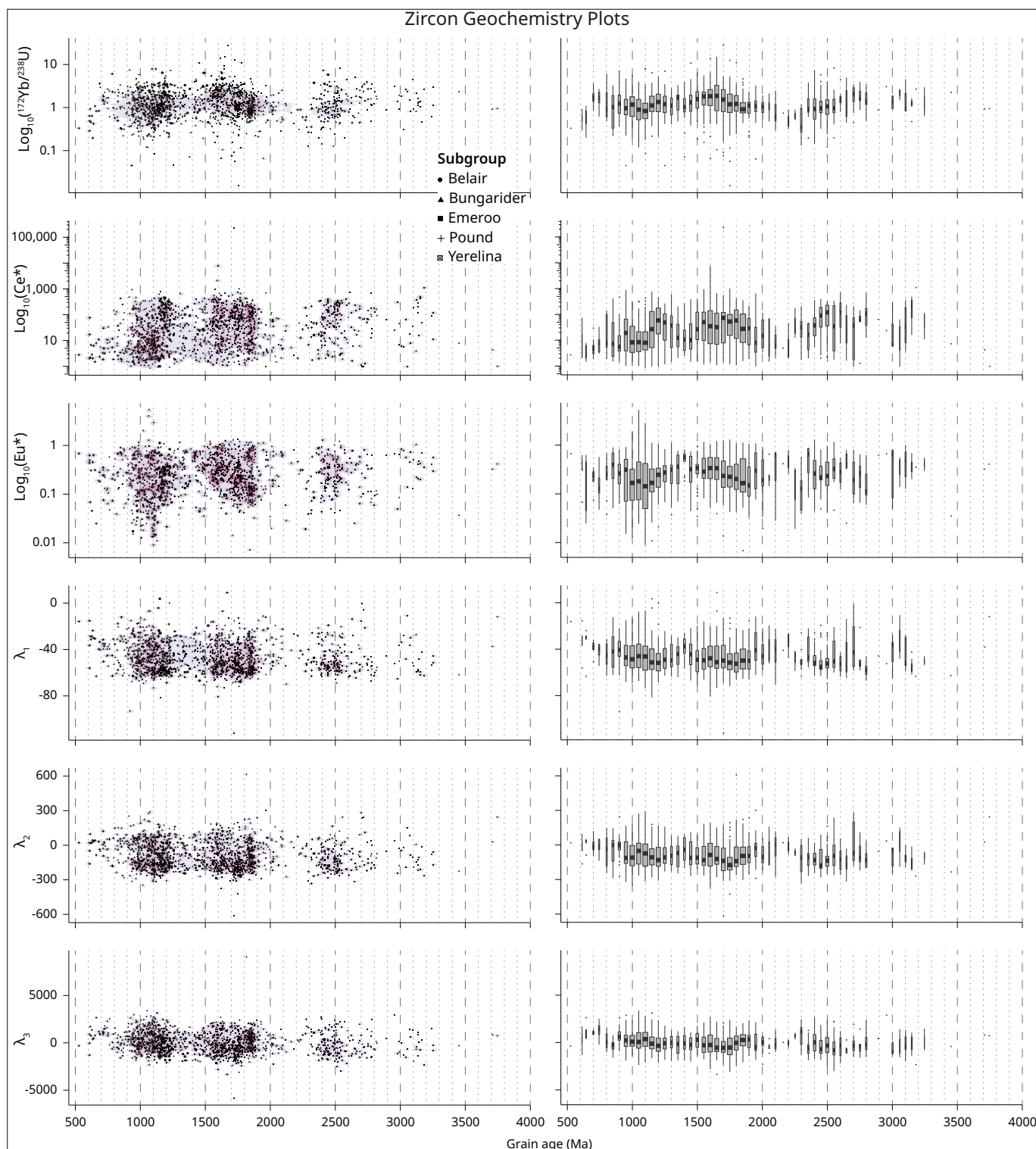


Figure 8 – Key zircon geochemistry plots for zircon analysed in this study. Left: Scatter plots underlain with 2D density estimation. Right: 50-million-year binned boxplots with width scaled by the count of values in the bin. Top to bottom: Yb/U, Ce*, Eu* and λ_{13} . λ_{13} are measures of lanthanoid pattern shapes, with λ_{13} representing the linear slope, quadratic slope, and cubic slope respectively. Ce*, Eu* and λ_{13} are calculated using BLambdaR (Anenburg and Williams, 2022).

of 798 ± 5 Ma and 799 ± 4 Ma (Fabris et al., 2005). The youngest limit for deposition of the Burra Group is poorly constrained as no volcanogenic sequences have been found to date in the upper Burra Group. Currently, the best constraints are MDAs obtained for both the Gilbert Range Quartzite (731 ± 34 Ma, Keeman et al., 2020; revised in Lloyd et al., 2020) and the Mitcham Quartzite (720 ± 21 Ma, Van der Wolff,

2020) of the Belair Subgroup. These MDAs, combined with those of the Sturt Formation, 714 ± 28 Ma, 698 ± 12 and 663 ± 11 Ma (Keeman et al., 2020; Lloyd et al., 2020, 2023), closely align with the time band defined globally for the Sturtian Glaciation (Rooney et al., 2015). As such, it is likely the younger limit for timing of deposition of the Burra Group is c. 717 Ma.

The Emeroo Group samples are of the

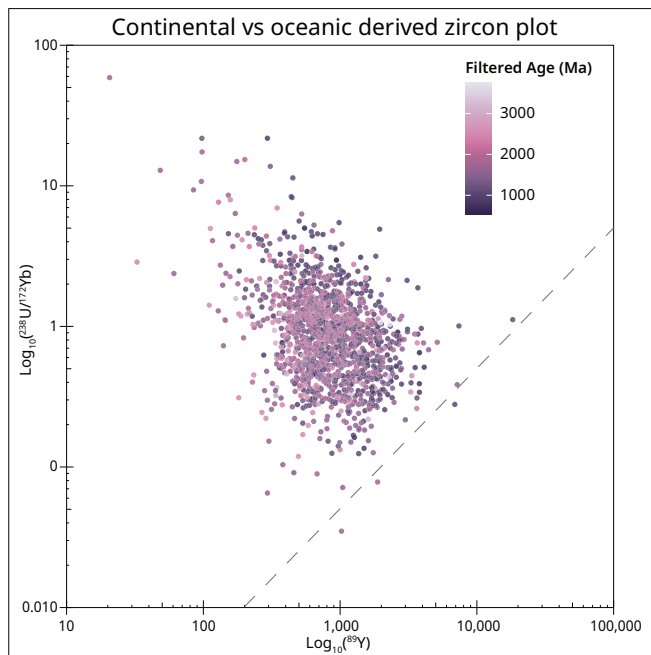


Figure 9 – Plot based used as an indicator of zircon crustal origin (Grimes *et al.*, 2007). This plots Y against U/Yb, with the dashed reference line dividing the “oceanic” (below line) and “continental” (above line) fields. Most data plot above the reference line, suggesting zircon formation mostly in crust of continental affinity. Coloured by filtered age where light is older and darker is younger.

Humanity Seat Formation (FR3_036), the Blue Mine Conglomerate (FR3_035), the Opaminda Formation (FR2_396), the Wortupa Quartzite (FR3_010), and the Copley Quartzite (FR3_123, FR2_002_01, & FR2_004_01). They were deposited between 802 ± 10 Ma and c. 790 Ma. The obtained MDAs for these samples were 1558 ± 35 Ma, 1079 ± 17 Ma, 1374 ± 21 Ma, 845 ± 13 Ma, 864 ± 16 Ma, 1195 ± 20 Ma, and 838 ± 13 Ma, respectively. All these MDAs are older than their expected depositional ages (<802 \pm 10 Ma, >c. 790 Ma)

Bungarider and Belair Subgroup samples were deposited after those of the Mundallio Subgroup, c. 790 Ma, and likely before c. 714 Ma, with the Belair Subgroup being the stratigraphically younger of the two. The Myrtle Springs Formation (North Flinders Ranges) sample, FR3_082a, has an MDA of 807 ± 16 Ma. The Saddleworth Formation sample, FRX_002 (South Flinders Ranges), has an MDA of 948 ± 15 Ma, and while data are extremely limited, sample FR1_006_03 (North Mount Lofty Ranges), has an MDA of 1562 ± 27 Ma. The MDA derived for sample FRX_002 is significantly older than the youngest grain quoted in the results section above, this is due to the more conservative criteria used here to define the MDA (i.e., within 2% of concordance). The final Bungarider Subgroup sample is from the Stonyfell Quartzite, SF1 (South Mount Lofty Ranges), and has an MDA of 1585 ± 25 Ma. These are all considerably older than the expected depositional age of the Bungarider Subgroup.

Sample FRX_001 (South Mount Lofty Ranges) is from a sedimentary rock thought to be correlative to the Gilbert Range Quartzite. Zircon yield was low for this sample with an MDA of 1101 ± 17 Ma obtained. Gilbert Range Quartzite sample, FR1_003_01 (North Mount Lofty Ranges), has an MDA of 869 ± 14 Ma. The final Burra Group sample in this study comes from the Mitcham Quartzite, sample ML_008 (South Mount Lofty Ranges). This was a second run on the sample to add additional data and for verification purposes of the MDA obtained in *Van der Wolff* (2020). An MDA of 730 ± 14 Ma ($^{206}\text{Pb}/^{238}\text{U}$) was obtained for the analyses in this study. Comparatively, the MDA quoted by *Van der Wolff* (2020) was 720 ± 21 Ma ($^{206}\text{Pb}/^{238}\text{U}$).

5.2.2 Umberatana Group

The three samples from the upper Umberatana Group (Yerelina Subgroup) were deposited during the onset (FR3_0111a, Fortress Hill Formation), maxima (FR3_089a, Mount Curtis Tillite), and deglaciation (FR3_088a, Balparana Sandstone) of the Marinoan Glaciation. All samples had low zircon yield, with FR3_088a being extremely low; the sample was a highly silicified, very-coarse arkose. The MDA for sample FR3_0111a is 976 ± 15 Ma, for sample FR_089a is 986 ± 18 Ma, and for sample FR3_088a is 944 ± 14 Ma.

No firm radiometric age constraints have been determined from within the Adelaide Superbasin on the Yerelina Subgroup representing the Marinoan Glaciation. Rose *et al.* (2013) obtained an MDA of 641 ± 5 Ma for the stratigraphically correlative Whyalla Sandstone on the Stuart Shelf. Additionally, Re-Os ages have provided a minimum age estimate for the interglacial Tapley Hill Formation of the Nepouie Subgroup c. 642 Ma (*Kendall et al.*, 2006), with a maximum constraint from a detrital zircon of 654 ± 13 Ma (*Lloyd et al.*, 2020). The Nepouie Subgroup is overlain by the Upalina Subgroup, which in turn underlies the Yerelina Subgroup, as such there is likely a reasonable amount of time between this constraint and the initial deposition of the Yerelina Subgroup. Globally, the Marinoan Glaciation is constrained to a younger limit c. 635 Ma (*Calver et al.*, 2013; *Rooney et al.*, 2015), while the older limit is not well defined. As such, the expected depositional age of the Yerelina Subgroup should be c. 645 to c. 635 Ma.

5.2.3 Wilpena Group

Sample FR3_095a is from the upper portion of the Bonney Sandstone. An MDA of 610 ± 9 Ma was obtained for this sample. Previously an MDA of 579 ± 32 Ma was obtained for the Bonney Sandstone (*Lloyd et al.*, 2020).

Additional zircons were analysed from samples 319 (Rawnsley Quartzite) and 058 (Billy Springs Formation) of *Lloyd et al.* (2020) to gain some trace element geochemistry for these samples. Only a

few zircons were remaining on sample 319, with an MDA of 1091 ± 22 Ma obtained from this limited data set. The MDA for sample 058 for this analytical session is 620 ± 10 Ma. Previous MDAs for these formations are 570 ± 23 Ma, and 564 ± 25 Ma, respectively. In sample 058, no grains younger than 620 ± 10 Ma for this analytical session are within 2% of concordance and thus are not considered reliable for MDA determination.

5.3 Provenance

Archaean zircons present in the detrital spectra (Figure 6) of all samples are consistent with being derived from local sources within the Gawler Craton (Figure 1) and recycling of detrital material from the Willyama Supergroup of the Curnamona Province (Figures 1 and 10). Numerous magmatic events occurred within the Gawler Craton at c. 3250 Ma, 3150 Ma, 2820 Ma, and 2560–2470 Ma, and inherited/detrital zircon up to 3400 Ma are present throughout the terrane (Fanning, 2007; Fraser and Neumann, 2010; Fraser et al., 2010; Jagodzinski et al., 2020, 2023; Jagodzinski and McAvaney, 2017; Reid and Jagodzinski, 2011; Williams and Reid, 2021). The Willyama Supergroup in the Curnamona Province contains detrital populations c. 3000–2980 Ma, and c. 2680–2650 Ma (Page et al., 2005), while their initial origin may be the North Australian Craton (Figure 1) (e.g. Barovich and Hand, 2008). All but one zircon of Archaean age is feasibly attributed to these local sources. One zircon present within the Mitcham Quartzite has an Eoarchaean age of c. 3746 Ma. The time resolved analysis of this zircon revealed two distinct zones of Pb and Pb/Th ratios, and REE concentrations. Both integration periods resolve ages c. 3700 Ma, with the latter part of the signal (~10s) resolving a nearly perfectly concordant measurement. Regardless of this complexity that is likely a result of inclusions, the age of this zircon can be confidently resolved as being mid-Eoarchaean.

Palaeoproterozoic zircons are ubiquitous throughout all samples but become increasingly less common up stratigraphy (Figure 6). The first consistently recorded population is late Archean to early Palaeoproterozoic, c. 2510–2400 Ma. These ages correlate well with the Sleaford Orogeny of the Gawler Craton (Reid et al., 2014). The most prominent Palaeoproterozoic zircon population occurs c. 1800–1600 Ma. Both the Gawler Craton and Curnamona Province (Figures 1 and 10) record abundant zircon of this age either as magmatic, metamorphic, or detrital components (Barovich and Hand, 2008; Belousova et al., 2009; Fanning, 2007; Fraser and Neumann, 2010; Jagodzinski and Fricke, 2010; Jagodzinski et al., 2020; Jagodzinski and McAvaney, 2017; McAvaney, 2012; Meaney, 2012, 2017; Morrissey et al., 2019; Reid et al., 2019; Reid and Hand, 2012; Reid and Jagodzinski, 2011; Reid and Payne, 2017; Swain et al., 2005). Another possible source is the Yavapai-Mazatzal Province of Laurentia (Figure 1) due to similarities in ages and proximity

to the Adelaide Superbasin within some Rodinia reconstructions (Brookfield, 1993; Dalziel, 1991; Goodge et al., 2008; Hoffman, 1991; Karlstrom, 1999; Karlstrom and Bowring, 1988; Moores, 1991; Wingate et al., 2002).

Early Mesoproterozoic zircon c. 1580 Ma forms a significant population (Figure 6) in older samples from the far northeast of the basin (Figure 2), especially in those from near the Mount Painter Inlier. It also forms a significant component of the Belair Subgroup samples in the far south of the basin (Figure 2). These are feasibly attributed to local derivation (Figure 10) from the Ninnerie Supersuite and Radium Creek Group (Armit et al., 2014; Wade, 2011), with additional potential sources being the Gawler Range Volcanics, Hiltaba Suite, and Barossa Complex of the Gawler Craton (Fanning, 2007; Meaney, 2017). A second Mesoproterozoic zircon population is present c. 1100 Ma. While generally absent from the older stratigraphic units (Figures 6 and 2), it becomes predominant in sample FR2_004_01 from the very top of the Copley Quartzite in the transitional section to the overlying Skillogee Dolomite. This is a notable change in population spectra from sample FR2_002_01 (Figures 6 and 10), which was sampled mid-Copley Quartzite in the same stratigraphic section. While Stenian zircon is almost absent in the two additional Copley Quartzite samples from this study (Figure 6), and from the samples presented in Lloyd et al. (2020), this is most likely because of stratigraphic height of sampling. This Stenian population is also present, but not as predominant in the coeval Wortupa Quartzite. In the overlying Skillogee Dolomite, there are significant variations in the population spectra (Figure 6 and 10) dependant on sample location. In the far northeast of the basin, the Calymmian population (c. 1580 Ma) remains the principal signature with a minor contribution from late Mesoproterozoic zircon, while in the Willouran Ranges to the northwest, Stenian zircon (c. 1100 Ma) are abundant. To the south, roughly in the middle of the basin, Stenian zircon are almost entirely absent from the Koorunga Member of the Skillogee Dolomite. The Myrtle Springs Formation sample from the middle (west–east) of the North Flinders Ranges (Figure 2 and 3) forms a single population peak centred on the Stenian-Tonian boundary, with only minor but consistent contributions from older source material (Figure 6). In the south of the basin this influx of latest Mesoproterozoic zircon occurs in a higher stratigraphic position, between the lower Bungarider Subgroup (the Stonyfell Quartzite) and Belair Subgroup (the Mitcham Quartzite) (Figure 6). The Saddleworth Formation samples from the middle of the basin appear to reflect these trends (Figure 6). The rather significant changes in DZ age spectra in the mid to upper Burra Group (Figure 10) strongly suggest an increasingly restricted, but more distal source region, the Musgrave Province (Figure 1) (Howard et al., 2015; Smithies et al., 2008, 2011; Smits

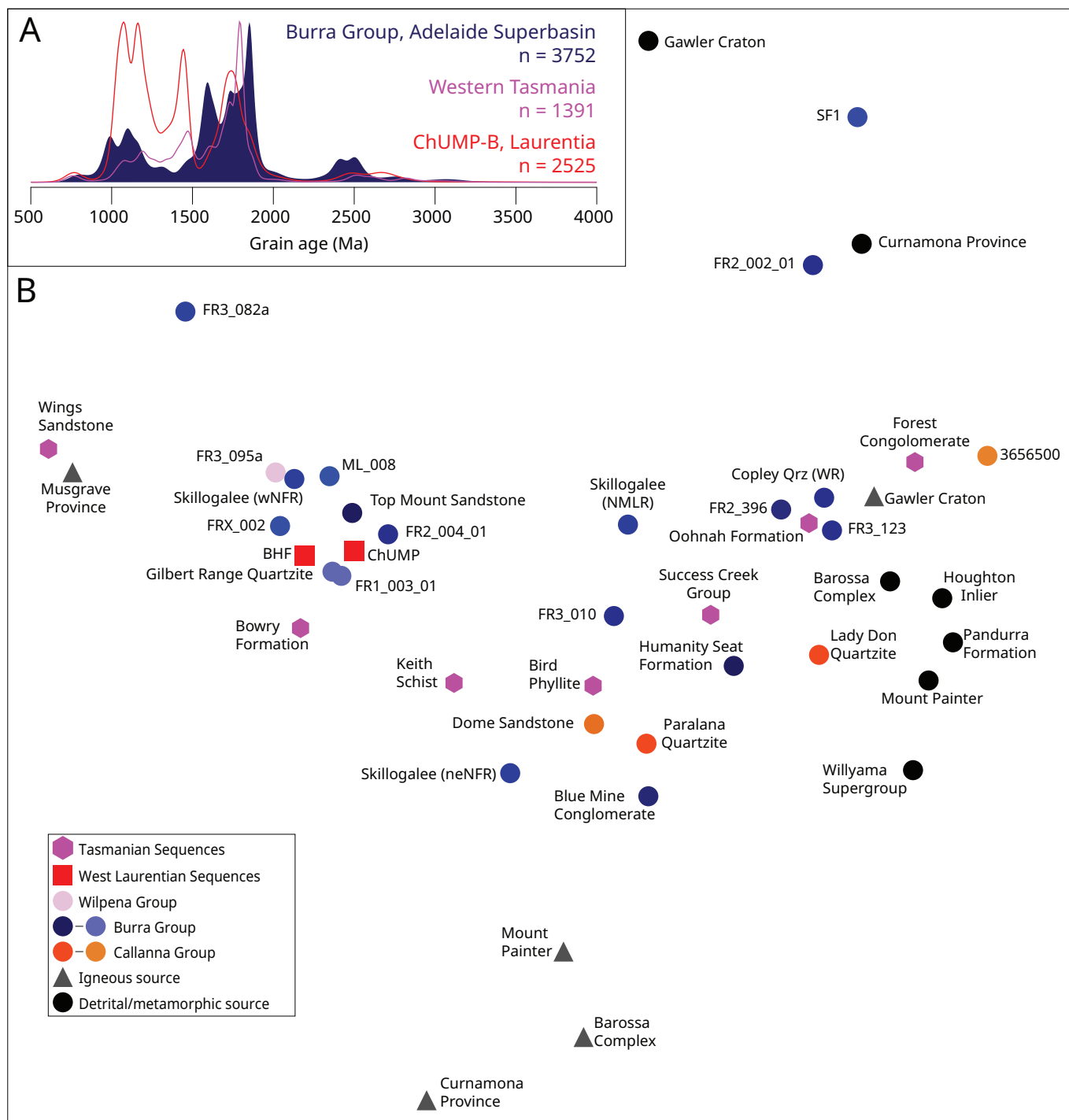


Figure 10 – A) Overlain KDEs of Tonian sequences of the Adelaide Superbasin (Burra Group: this study; *Keeman et al., 2020; Lloyd et al., 2020; Van der Wolff, 2020*), western Laurentia (Chaur, Uinta Mountain, middle Pahrump Groups–Buffalo Hump Formation correlated rocks (ChUMP-B); *Brennan et al., 2021; Dehler et al., 2017*) and the Western Tasmania Terrane (*Mulder et al., 2018b, 2020*). **B)** Non-metric multidimensional scaling plot of samples analysed ($n > 40$) in this study (blue coloured circles, pink circle) with data from underlying Adelaide Superbasin rocks (orange circles, *Brotodewo et al., 2021; Lloyd et al., 2020*), potential correlative formations in Tasmania (magenta hexagons), western Laurentia (red squares), and potential source regions for the Adelaide Superbasin rocks (black and grey circles and triangles). This plot shows relative similarity of all data to each other and are intended as a visual guide. Points that are closer together suggest greater similarity. For data of the Adelaide Superbasin, the lightness of colour corresponds to stratigraphic position, i.e., lighter shade are younger rocks. Axes are omitted as the algorithm used produces normalised values with no physical meaning and can be safely removed. Produced using IsoplotR which uses the Kolmogorov-Smirnov statistic for computation of the MDS (*Vermeesch, 2018*).

et al., 2014; Wade et al., 2008), as has been inferred in past studies (*Keeman et al., 2020; Lloyd et al., 2020*). One alternate source is the Albany-Fraser Orogen (Figure 1) of Western Australia (*Spaggiari*

et al., 2015). However, this would require transport across the Gawler Craton at the same time as deposition was occurring in the western Officer Basin (Figure 1) (*Zi et al., 2019*). In addition, coeval, c.

750–720 Ma, uplift of the Musgrave Province has been interpreted to occur (Howard *et al.*, 2015) and, the abrupt up-sequence spectra change in the two Copley Quartzite samples (Figures 6 and 10) from the Copley area (Figure 3) suggests that the Gawler Craton was somewhat restricted as a source region, effectively precluding the Albany–Fraser Orogen as a source. Antarctic (Figure 1) sources are also possible, where the late Mesoproterozoic/early Tonian zircon in the Palaeozoic Lachlan Orogen is thought to be derived from (Squire *et al.*, 2006). A distinguishing feature of these Lachlan Orogen zircons is the significant amount of <1050 Ma zircon, these are more characteristic of parts of East Antarctica such as the Tonian Oceanic Arc Super Terrane (TOAST, Jacobs *et al.*, 2015, 2017) and the Rayner Complex (Fitzsimons, 2000). The South Tasman Rise (Figure 1) is another possible source for late Mesoproterozoic to early Neoproterozoic zircon (Berry *et al.*, 2008; Fioretti *et al.*, 2005), as is the hypothesised Precambrian keel of Zealandia (Adams and Campbell, 2023; Adams and Ramsay, 2022; Turnbull *et al.*, 2021). U–Pb DZ ages from the Myrtle Springs Formation, the Mitcham Quartzite, and the Gilbert Range Quartzite samples appear to support an influx of younger, more exotic detritus (Figure 6).

Tonian zircons are almost entirely absent from the Emeroo Subgroup stratigraphy in the north of the basin, and are absent from all Emeroo to mid-Bungarider Subgroup rocks in the far south of the basin near Adelaide (Figures 6 and 2) (this study; Van der Wolff, 2020). The presence of Neoproterozoic zircon in Burra Group sequences generally coincides with the introduction of Stenian zircon, the exception being the Koorunga Member of the Skilloogalee Dolomite (Figure 6) where syndepositional magmatism is recorded (Preiss *et al.*, 2009). For the most part, Tonian zircons within the Burra Group sequences are c. 1000–780 Ma in age, with a minor amount of zircon with ages 760–730 Ma in the Mitcham Quartzite (Figure 6). Zircon aged c. 830–780 Ma is probably derived locally from the early magmatism recorded in the Callanna Group, and lower Burra Group (Armistead *et al.*, 2020; Fanning *et al.*, 1986; Preiss *et al.*, 2008, 2009; Wingate *et al.*, 1998). Zircons with ages between c. 1000 Ma and 890 Ma, and c. 760–730 Ma are more enigmatic. While earlier zircon aged c. 1000 Ma may be attributable to the Musgrave Province where some bimodal magmatism is recorded (Howard *et al.*, 2015), the reasonably significant number of concordant zircons between 980 and 900 Ma are much more difficult to reconcile with current data from the Musgrave Province. Burra Group c. 760–730 Ma DZs have only been found in the Mitcham Quartzite. While a few grains of these ages are in the dataset for the Saddleworth Formation they are likely to be artefacts of radiogenic Pb loss or inclusions affecting the U–Pb age determinations and are not considered reliable. Few sources of c. 760–730 Ma zircon are known within Proterozoic Australia. Poorly constrained

age determinations of 768 ± 9 Ma and 764 ± 42 Ma (K–Ar dating of plagioclase) were obtained from mafic volcanics of the Poldas Basin just to the west of the Adelaide Superbasin (Flint *et al.*, 1988). In the southwestern Pilbara Region of Western Australia an age of 755 ± 3 Ma was determined for the Mundine Well Dolerite by U–Pb analysis of zircon and baddeleyite (Wingate and Giddings, 2000), while the Keene Basalt in the western Officer Basin has been dated at 753.04 ± 0.84 Ma, and 752 ± 4 Ma by $^{40}\text{Ar}/^{39}\text{Ar}$ determinations of plagioclase and pyroxene respectively (Zi *et al.*, 2019). An age of 731 ± 0.2 Ma has been resolved from zircon of the Mud Tank Carbonatite in the Strangways Range, Northern Territory (Black *et al.*, 1978; Gain *et al.*, 2019). Mulder *et al.* (2020) summarised several Tonian magmatic ages from Tasmania, these being c. 775 Ma, 760 Ma, 748 Ma, and 733 Ma. However, in their model western Tasmania is located at the south-eastern edge of East Antarctica (Figure 1). Given the low abundance of these zircon in the Mitcham Quartzite, and lack of zircon of this age in northern samples (Figure 6) it would suggest that they are not derived from the north-westerly sources, and are more likely derived from either local, low volume magmatism, or more distal southerly sources—potentially western Tasmania (e.g. the c. 775–750 Ma granitoids on King Island).

South China and Tarim contain magmatic records of Tonian zircon c. 1000 Ma to c. 700 Ma (Cawood *et al.*, 2018, 2020; Hui *et al.*, 2021; Lan *et al.*, 2015; Shu *et al.*, 2021; Wu *et al.*, 2021) and have both been previously invoked as “missing-links” within central Rodinia between Australia–Laurentia (Li *et al.*, 1995, 2008; Wen *et al.*, 2017, 2018). However, we do not consider these to be viable source regions for the Adelaide Superbasin for several reasons. A growing consensus of researchers (Cawood *et al.*, 2020; Eyster *et al.*, 2020; Park *et al.*, 2021; Wu *et al.*, 2018, 2021; Zhang *et al.*, 2019; Zhao *et al.*, 2021; Zheng *et al.*, 2020; Zhou *et al.*, 2021) have independently drawn conclusions that these two terranes are either on the periphery of, or detached from, Rodinia. This is supported by multiple lines of geologic evidence including palaeomagnetic studies, detrital zircon studies, and more holistic tectonic evolution models for these terranes involving multiple methods (e.g. Merdith *et al.*, 2019). Given that South China and Tarim appear to record a prolonged and semi-continuous record of accretionary tectonics (e.g. arcs, ophiolites, blueschists: Tang *et al.*, 2016; Zhang *et al.*, 2015; Zhou *et al.*, 2022) it would support the belief that these two terranes were on the periphery of Rodinia, as these long-lived accretionary tectonic systems are hard to justify in the central area of a supercontinent.

Cryogenian to Ediacaran zircons are abundant in the Yerelina and Pound Subgroup samples and have been addressed in Lloyd *et al.* (2020). The results obtained in this study, even though generally limited in number, conform to earlier results (Figure 6), and

the ultimate source of these zircon remains enigmatic aside from some local magmatism c. 660 Ma (Cox et al., 2018) and c. 580 Ma (Black, 2007). Notably this population of zircon is present further afield in Tasmania within the Cottons Breccia and on King Island (Calver et al., 2013), and within Cryogenian strata of northwest Tasmania (Mulder et al., 2020). Felsic magmatic sources c. 650 Ma are known to be present within the Trans-Antarctic rift margin sequences (Cooper et al., 2011), and these may be a potential source for both the Tasmanian and South Australian rocks (Figure 1).

Interestingly, both the Skilloalee Dolomite samples (Lloyd et al., 2020) from the Willouran Ranges and the Myrtle Springs Formation sample have a considerable number of post 1030 Ma zircon, with the most predominant population peak c. 1000–990 Ma for both samples (Figure 6). Additionally, Mesoproterozoic zircon in the Myrtle Springs Formation sample appears to not reflect the typical bimodal (c. 1220–1150 Ma & 1090–1040 Ma) Musgrave Province signature (Howard et al., 2015; Johansson et al., 2022). While not precluding detritus derived from the Musgrave Province, it does suggest an alternate source may have been involved. Given the consistency of zircon populations in Emeroo to mid-Bungarider Subgroup in the very south of the basin (Van der Wolff, 2020), and the lack of late Mesoproterozoic to early Tonian zircon in the Skilloalee Dolomite from the North Mount Lofty Ranges (Figure 6), it effectively rules out a southerly source for these. This suggests an unrecognised source to the north or northeast of the Adelaide Superbasin. Contrastingly, younger Pound Subgroup zircon populations (Figure 6) are more easily reconciled as being primarily derived from the Musgrave Province (Figure 10) with other additional sources, likely to the south, accounting for Cryogenian to Ediacaran zircon populations (Lloyd et al., 2020).

5.4 Comparison to Palaeocurrent Data

Palaeocurrent data for the Burra Group remains limited; however, the two studies using palaeocurrent data (Uppil, 1980; Virgo et al., 2021) have both suggested primarily south-southeast directed current flow along the north-western margin of the basin. This supports transportation from the northwest of the basin as suggested by detrital zircon data. Unfortunately, there is a distinct lack of palaeocurrent data from the north-eastern Tonian strata. Palaeocurrent data for the Cryogenian strata in the northern region of the Adelaide Superbasin was addressed in (Lloyd et al., 2023), and broadly agreed with the detrital zircon data presented in that research. Ediacaran strata have been studied in greater detail regarding palaeocurrent directions (e.g. Gehling, 1982; Counts and Amos, 2016), noting that deposition (in the northern regions) at this time was primarily in fluvial-deltaic environments, with detritus ultimately sourced northwest of

the basin system. However, salt tectonics active during deposition of the Burra Group and into the Cambrian (Rowan et al., 2020) influenced local areas, thus some palaeocurrent directions may reflect diapir-generated slopes and sediment transport, and not the overall basin palaeogeography.

5.5 Comparison to Tasmanian and Laurentian Sequences

Along with North China and eastern Proterozoic Australia, both the Western Tasmania Terrane (WTT) and western Laurentia are witness to the opening of the proto-Pacific Ocean during the breakup of Rodinia (Figure 1) (Brennan et al., 2021; Merdith et al., 2021; Mulder et al., 2020). As such, the stratigraphic sequences recorded in these rift basins are crucial to better understanding the configuration of these continental blocks within the heart of Rodinia. Mulder et al. (2020) suggest three potential positions for the WTT at c. 730 Ma, one against southeast East Antarctica, and two against western Laurentia. A comparison of the U–Pb DZ spectra of coeval sedimentary sequences in these terranes provides insights into their relative positions and links. The coeval sedimentary sequences of the Burra Group in the WTT are the Bowry Formation, the Keith Schist, the Forest Conglomerate, the Bird Phyllite, the Success Creek Group, the Oonah Formation, and potentially the Wings Sandstone (Mulder et al., 2018b, 2020). In western Laurentia (Figure 1) the coeval sequences are the ChUMP-B (Chaur, Uinta Mountain, middle Pahrump Groups–Buffalo Hump Formation) correlated rocks (Brennan et al., 2021; Dehler et al., 2017). The Windermere Supergroup and Mackenzie Mountains Supergroup (Strauss et al., 2015) have long thought to be correlatives of the Adelaidean sequences (Young and Gostin, 1991). The more nuanced complexity of the geological history and detrital zircons of these rocks from the WTT and western Laurentia are detailed in their respective publications. The combined DZ age distributions of the late Tonian ChUMP-B, WTT, and Burra Group rocks are overlain on the inset of Figure 10, and while they do show significant similarities, some key differences appear. The most obvious differences are the position of the latest Palaeoproterozoic peaks, the relative lack of earliest Mesoproterozoic zircon in the WTT and ChUMP-B spectra, and the position of the latest Stenian to early Tonian peaks. In the datasets available, WTT rocks show remarkable similarity to the ChUMP-B populations, closely following the general trends, albeit in different relative proportions. The combined spectra suggest, that overall, WTT has a stronger affinity with western Laurentia than it does southeast Proterozoic Australia, but all terranes share some similar-aged sources. However, the individual WTT sequences plot (on an MDS) with an inverse stratigraphic relationship to detrital zircon similarity of the western Laurentian data—that is they become increasingly dissimilar up-sequence (Figure 10). The Tonian strata in

Tasmania are interpreted to be largely recycled from the underlying Mesoproterozoic Rocky Cape Group (Mulder *et al.*, 2020), which is thought to correlate with Mesoproterozoic sequences in western Laurentia (Halpin *et al.*, 2014; Mulder *et al.*, 2015, 2018a). However, additional igneous and metasedimentary sources from the Mawson Continent (Figure 1) (Goodge *et al.*, 2017; Williams *et al.*, 2018) may also be involved as these closely align with the zircon distribution of western Laurentia and Tasmania. The latter observation, combined with the general paucity of Stenian detrital zircon in Tonian sequences of Tasmania, which are abundant in time-equivalent upper ChUMP-B rocks, would suggest that the WTT remained a part of Australia-Antarctica, on the western side of the proto-Pacific. This allows for the late Tonian magmatism recorded in the WTT to be a potential source of the enigmatic c. 760–730 Ma zircons found in the Belair Subgroup of the Adelaide Superbasin. Contrastingly, generally younger Burra Group rocks show greater similarity (Figure 10) to the ChUMP-B strata. We suggest that this is likely due to the greater Stenian zircon populations present in the upper Burra Group derived from the Musgrave Province, and a potentially intervening terrane to the north/northeast of the basin (discussed above) rather than a shared source in the very latest Tonian.

Unfortunately, no U–Pb DZ data from the Burra Group rocks in the far east of the basin have been obtained to date, and little is known of what lies beneath the Warburton Basin to the north. This significantly hinders the ability to understand the links between eastern Proterozoic Australia and western Laurentia or any intervening terrane (Figure 1).

5.6 Tectonic and Palaeogeographic Implications

It is evident that tectonics played a significant role during the deposition of the Burra Group. Significant and rapid changes in thickness and lithology (Figure 5), both vertically and laterally throughout the basin (Preiss, 1987, 1993, 2000; Uppil, 1980), suggest the development of numerous half-graben depocentres, as do abrupt up-sequence changes in DZ age populations (Figures 10 and 6). For example, in the north of the basin there is abrupt change in U–Pb DZ spectra at the Emeroo–Mundallio Subgroup boundary (Figures 10 and 6). The boundary marks a significant decrease in DZ with ages characteristic of the Gawler Craton, and a corresponding increase in zircon thought to be derived from the Musgrave Province. We suggest that this transition marks the uplift of rift shoulders at c. 800–790 Ma, effectively funnelling detrital material through the rift valley from the northeast and physically blocking much of the detrital material from the interior of the Gawler Craton. Interestingly, DZ ages shift to a latest Stenian to early Tonian population in the Myrtle Springs Formation (Figure 6). Currently the source(s) of these zircons are unknown,

but it is likely to be from the north or northeast. This is based upon the uniformity of equivalent strata in the south of the basin reflecting purely local derivation from older Palaeoproterozoic to early Mesoproterozoic sources (Van der Wolff, 2020), and the sequences in the middle of the basin reflecting the same observation, with the addition of c. 790–780 Ma from local sources.

A similar abrupt transition in DZ age spectra (Figures 10 and 6) occurs much higher in the stratigraphy in the southern and middle areas of the basin, between deposition of the upper Bungarider Subgroup (the Saddleworth Formation) and the lower Belair Subgroup (the Mitcham Quartzite). These observations suggest a southward advancement of the rift system in the Adelaide Superbasin, with main pulses of extension occurring c. 790 Ma in the northern to middle (and likely eastern) areas of the basin, and sometime around 750–730 Ma in the southern and middle areas of the basin. The older c. 790 Ma extension has a known magmatic record within the Adelaide Superbasin (Armistead *et al.*, 2020; Preiss, 1987; Preiss *et al.*, 2009), while the younger extension appears to be amagmatic. It is also likely that rift shoulders were well developed by c. 750–730 Ma for the entire Adelaide Rift Complex as Palaeoproterozoic and older zircon characteristic of the Gawler Craton are only present in relatively minor amounts in the upper Burra Group sedimentary rocks.

These findings are supportive of southward advancement of rift phases within the overall rift system along the eastern margin of late Proterozoic Australia–East Antarctica. Southward advancement of the rift phases is consistent with palaeogeographic and tectonic models of Merdith *et al.* (2021) and Mulder *et al.* (2020), and a likely continuation of the rift basin system under the modern-day Trans-Antarctic Mountains (Goodge, 2020) which is supported by the presence of mid-Neoproterozoic rift sequences with an apparent lack of earlier Tonian rift sequences (Cooper *et al.*, 2011).

6 Conclusions

This study significantly increases the quantity and diversity of detrital zircon U–Pb data from the Tonian rocks of the Burra Group in the Adelaide Superbasin, adding 1392 new analyses from eleven formations. We also present an additional contribution of 304 DZ U–Pb data from the Yerelina and Pound subgroups. We note abrupt changes in DZ U–Pb populations that occur at temporally different points across the basin, i.e. the abrupt changes occur lower in stratigraphy in the north of the basin. The sedimentology of these sequences is suggestive of tectonic controls on sediment inputs and the development of depocentres within the basin.

Our results indicate that two main pulses of extension occurred at c. 790–780 Ma in the north

and middle of, and c. 750–730 Ma in the south of, the Adelaide Superbasin, and that rift shoulders were well developed in the Adelaide Rift Complex by c. 730 Ma. We interpret our results to reflect a southward advancement of the rift system within the Adelaide Rift Complex (of the Adelaide Superbasin) during the late Tonian separation of the eastern margin of Australia–East Antarctica from Laurentia in Rodinia. Our data also provides a maximum depositional age constraint for the uppermost Burra Group (upper Belair Subgroup) from the Mitcham Quartzite of 730 ± 14 Ma, indicating that deposition of the Burra Group continued (in the southern Adelaide Superbasin) to near the beginning of the Sturtian Glaciation. Finally, we suggest that the Western Tasmania Terrane likely stayed on the western side of the proto-Pacific during the separation of Rodinia, and the possibility of an unrecognised source of c. 1000–900 Ma zircon to the north, or northeast of the Adelaide Superbasin.

Acknowledgements

We acknowledge the Adnyamathanha, Arabana, Banggarla, Kurna, Kokatha, Kuyani, Ngadjuri and Nukunu Peoples as the Traditional Owners and Custodians of the land on which this research is conducted. We acknowledge and respect their deep feelings of attachment and spiritual relationship to Country, and that their cultural and heritage beliefs are still as important to the living people today. The authors acknowledge the instruments and scientific and technical assistance of Microscopy Australia at Adelaide Microscopy, The University of Adelaide, a facility that is funded by the University, and State and Federal Governments. Particular thanks to Aoife McFadden for their assistance with CL imaging. We also thank Dr Wolfgang Preiss (Geological Survey of South Australia; University of Adelaide) for sharing his expertise on the Adelaide Superbasin, James Nankivell, and Georgina Virgo (University of Adelaide) for their assistance with fieldwork. Arkaroola Wilderness Sanctuary and Operation Flinders (Yankaninna Station) are thanked for their generous hospitality during fieldwork on their properties. This work is conducted with the appropriate permissions and scientific permits from the relevant stakeholders. This publication forms MinEx CRC document number 2024/25.

The Geological Survey of South Australia and the MinEx CRC funded this research. This research was supported by an Australian Government Research Training Program (RTP) Scholarship awarded to JCL.

Author contributions

Jarred C. Lloyd: Conceptualisation, investigation, writing - original draft, writing - review & editing, methodology, formal analysis, data curation, visualisation. **Alan S. Collins:** Conceptualisation, funding acquisition, supervision, investigation,

writing - review & editing. **Morgan L. Blades:** Investigation, writing - review & editing. **Sarah E. Gilbert:** Formal analysis, methodology, investigation, writing - review & editing. **Jacob A. Mulder:** Writing - review & editing. **Kathryn J. Amos:** Conceptualisation, funding acquisition, supervision, writing - review & editing.

Data availability

Complete data for this publication are freely available for download from Figshare at the following links. These datasets contain all the U–Pb geochronology data, trace element data, and basic sample metadata. Zircon and NIST standards data for all analytical sessions: doi.org/10.6084/m9.figshare.18131432. Burra Group, Yerelina Subgroup, and Pound Subgroup detrital zircon data (this study): doi.org/10.6084/m9.figshare.1915060. Zircon CL images: doi.org/10.6084/m9.figshare.19181024. R code used to generate the zircon geochemistry plots is available on GitHub at github.com/jarredclloyd/zircon-trace-element-plots.

Competing interests

The authors declare no competing interests.

Peer review

This publication was peer-reviewed by Peter Cawood and Mauro Geraldes. The full peer-review report can be found here: tektonika.online/index.php/home/article/view/65/104

Copyright notice

© Author(s) 2024. This article is distributed under the [Creative Commons Attribution 4.0 International License](https://creativecommons.org/licenses/by/4.0/), which permits unrestricted use, distribution, and reproduction in any medium, provided the original author(s) and source are credited, and any changes made are indicated.

References

- Adams, C. J., and H. J. Campbell (2023), Zealandia and Australia at Ordovician continental margins: reconciling their similar and differing detrital zircon provenances within Rodinia, *New Zealand journal of geology and geophysics*, 66(3), 456–477, doi: [10.1080/00288306.2023.2197238](https://doi.org/10.1080/00288306.2023.2197238).
- Adams, C. J., and W. R. H. Ramsay (2022), Archean and Paleoproterozoic zircons in Paleozoic sandstones in southern New Zealand: evidence for remnant Nuna supercontinent and Ur continent rocks within Zealandia, *Australian journal of earth sciences*, 69(8), 1061–1081, doi: [10.1080/08120099.2022.2091039](https://doi.org/10.1080/08120099.2022.2091039).
- Anenburg, M., and M. J. Williams (2022), Quantifying the tetrad effect, shape components, and Ce–Eu–Gd anomalies in rare earth element

- patterns, *Mathematical geosciences*, 54(1), 47–70, doi: 10.1007/s11004-021-09959-5.
- Armistead, S. E., A. S. Collins, S. Buckman, and R. Atkins (2020), Age and geochemistry of the boucaut volcanics in the neoproterozoic Adelaide rift complex, south Australia, *Australian journal of earth sciences*, 64(4), 1–10, doi: 10.1080/08120099.2021.1840435.
- Armit, R. J., P. G. Betts, B. F. Schaefer, M. J. Pankhurst, and D. Giles (2014), Provenance of the Early Mesoproterozoic Radium Creek Group in the northern Mount Painter Inlier: Correlating isotopic signatures to inform tectonic reconstructions, *Precambrian research*, 243, 63–87, doi: 10.1016/j.precamres.2013.12.022.
- Barovich, K., and M. Hand (2008), Tectonic setting and provenance of the Paleoproterozoic Willyama Supergroup, Curnamona Province, Australia: Geochemical and Nd isotopic constraints on contrasting source terrain components, *Precambrian research*, 166(1–4), 318–337, doi: 10.1016/j.precamres.2007.06.024.
- Belousova, E. A., A. J. Reid, W. L. Griffin, and S. Y. O'Reilly (2009), Rejuvenation vs. recycling of Archean crust in the Gawler Craton, South Australia: Evidence from U–Pb and Hf isotopes in detrital zircon, *Lithos*, 113(3–4), 570–582, doi: 10.1016/j.lithos.2009.06.028.
- Berry, R. F., D. A. Steele, and S. Meffre (2008), Proterozoic metamorphism in Tasmania: Implications for tectonic reconstructions, *Precambrian research*, 166(1–4), 387–396, doi: 10.1016/j.precamres.2007.05.004.
- Betts, M. J., J. R. Paterson, S. M. Jacquet, A. S. Andrew, P. A. Hall, J. B. Jago, E. A. Jagodzinski, W. V. Preiss, J. L. Crowley, S. A. Birch, C. P. Mathewson, D. C. García-Bellido, T. P. Topper, C. B. Skovsted, and G. A. Brock (2018), Early Cambrian chronostratigraphy and geochronology of South Australia, *Earth-science reviews*, 185, 498–543, doi: 10.1016/j.earscirev.2018.06.005.
- Black, L., B. Lp, and G. Bl (1978), The age of the mud tank carbonatite, strangways range, northern territory, *BMR journal of Australian geology and geophysics*, 3, 227–232.
- Black, L. P. (2007), SHRIMP U–Pb zircon ages obtained during 2006/07 for NSW Geological Survey Projects, *Tech. rep.*, Geological Survey of New South Wales, Australia.
- Bobrovskiy, I., J. M. Hope, A. Ivantsov, B. J. Nettersheim, C. Hallmann, and J. J. Brocks (2018), Ancient steroids establish the Ediacaran fossil Dickinsonia as one of the earliest animals, *Science (New York, N.Y.)*, 361(6408), 1246–1249, doi: 10.1126/science.aat7228.
- Brennan, D. T., Z.-X. Li, K. Rankenburg, N. Evans, P. K. Link, A. R. Nordsvan, C. L. Kirkland, J. B. Mahoney, T. Johnson, and B. J. McDonald (2021), Recalibrating Rodinian rifting in the northwestern United States, *Geology*, 49(6), 617–622, doi: 10.1130/g48435.1.
- Brookfield, M. E. (1993), Neoproterozoic Laurentia–Australia fit, *Geology*, 21(8), 683–686, doi: 10.1130/0091-7613(1993)021<0683:NLAf>2.3.CO;2.
- Brotodewo, A., T. W. Wise, and J. C. Lloyd (2021), LA-ICP-MS detrital zircon geochronology from the Delamerian Orogen, *Tech. rep.*, Geological Survey of South Australia, South Australia.
- Calver, C. R., J. L. Crowley, M. T. D. Wingate, D. A. D. Evans, T. D. Raub, and M. D. Schmitz (2013), Globally synchronous Marinoan deglaciation indicated by U–Pb geochronology of the Cottons Breccia, Tasmania, Australia, *Geology*, 41(10), 1127–1130, doi: 10.1130/G34568.1.
- Cao, X., A. Collins, S. Pisarevsky, N. Flament, S. Li, D. Hasterok, and R. Müller (2024), Earth's tectonic and plate boundary evolution over 1.8 billion years, *EarthArXiv*, doi: 10.31223/x5cw96.
- Cawood, P. A., G. Zhao, J. Yao, W. Wang, Y. Xu, and Y. Wang (2018), Reconstructing South China in Phanerozoic and Precambrian supercontinents, *Earth-science reviews*, 186, 173–194, doi: 10.1016/j.earscirev.2017.06.001.
- Cawood, P. A., W. Wang, T. Zhao, Y. Xu, J. A. Mulder, S. A. Pisarevsky, L. Zhang, C. Gan, H. He, H. Liu, L. Qi, Y. Wang, J. Yao, G. Zhao, M.-F. Zhou, and J.-W. Zi (2020), Deconstructing South China and consequences for reconstructing Nuna and Rodinia, *Earth-science reviews*, 204(103169), 103,169, doi: 10.1016/j.earscirev.2020.103169.
- Collins, A. S., S. M. Reddy, C. Buchan, and A. Mruma (2004), Temporal constraints on Palaeoproterozoic eclogite formation and exhumation (Usagaran Orogen, Tanzania), *Earth and planetary science letters*, 224(1–2), 175–192, doi: 10.1016/j.epsl.2004.04.027.
- Cooper, A. F., R. Maas, J. M. Scott, and A. J. W. Barber (2011), Dating of volcanism and sedimentation in the Skelton Group, Transantarctic Mountains: Implications for the Rodinia–Gondwana transition in southern Victoria Land, Antarctica, *Geological Society of America bulletin*, 123(3–4), 681–702, doi: 10.1130/B30237.1.
- Cooper, P. F., and K. D. Tuckwell (1971), The upper Precambrian Adelaidean of the Broken Hill area—a new subdivision, *Quarterly Notes of the Geological Survey of New South Wales*, 3, 8–16.
- Counts, J. W. (2017), The Adelaide Rift Complex in the Flinders Ranges: geologic history, past investigations and relevant analogues, *Tech. rep.*, Geological Survey of South Australia, Adelaide, South Australia.
- Counts, J. W., and K. J. Amos (2016), Sedimentology, depositional environments and significance of an Ediacaran salt-withdrawal minibasin, Billy Springs Formation, Flinders Ranges, South Australia, *Sedimentology*, 63(5), 1084–1123, doi: 10.1111/sed.12250.
- Counts, J. W., F. Rarity, R. B. Ainsworth, K. J. Amos, T. Lane, S. Morón, J. Trainor, C. Valenti, and R. Nanson (2016), Sedimentological interpretation of an Ediacaran delta: Bonney Sandstone, South Australia, *Australian journal of earth sciences*, 63(3), 257–273, doi: 10.1080/08120099.2016.1180322.
- Counts, J. W., C. R. Dalgarno, K. J. Amos, and S. T. Hasiotis (2019), Lateral facies variability along the margin of an outcropping salt-withdrawal minibasin, south Australia, *Journal of sedimentary research*, 89(1), 28–45, doi: 10.2110/jsr.2019.2.
- Cox, G. M., V. Isakson, P. F. Hoffman, T. M. Gernon, M. D. Schmitz, S. Shahin, A. S. Collins, W. Preiss, M. L. Blades, R. N. Mitchell, and A. Nordsvan (2018), South Australian U–Pb zircon (CA-ID-TIMS) age supports globally synchronous Sturtian deglaciation, *Precambrian research*, 315, 257–263, doi: 10.1016/j.precamres.2018.07.007.
- Dalziel, I. W. D. (1991), Pacific margins of Laurentia and East Antarctica–Australia as a conjugate rift pair: Evidence and implications for an Eocambrian supercontinent, *Geology*, 19(6), 598–601, doi: 10.1130/0091-7613(1991)019<0598:PMOLAE>2.3.CO;2.
- Danielson, J., and D. Gesch (2011), Global multi-resolution

- terrain elevation data 2010 (GMTED2010), *Tech. Rep. 2011-1073*, U.S. Geological Survey, doi: 10.3133/OFR20111073.
- Dehler, C., G. Gehrels, S. Porter, M. Heizler, K. Karlstrom, G. Cox, L. Crossey, and M. Timmons (2017), Synthesis of the 780–740 Ma Chuar, Uinta Mountain, and Pahrump (ChUMP) groups, western USA: Implications for Laurentia-wide cratonic marine basins, *Geological Society of America bulletin*, 129(5-6), 607–624, doi: 10.1130/B31532.1.
- Drexel, J. F. (2008), Review of the Burra Mine Project, 1980–2008—a progress report, *Tech. rep.*, Geological Survey of South Australia, South Australia.
- Drexel, J. F., and W. V. Preiss (1995), *The geology of South Australia, Bulletin*, vol. 2, The Phanerozoic, Geological Survey of South Australia, Eastwood, NSW, Australia.
- Dröllner, M., M. Barham, C. L. Kirkland, and B. Ware (2021), Every zircon deserves a date: selection bias in detrital geochronology, *Geological magazine*, 158(6), 1135–1142, doi: 10.1017/s0016756821000145.
- Eickhoff, K.-H., C. C. Von Der Borch, and A. E. Grady (1988), Proterozoic canyons of the Flinders Ranges (South Australia): submarine canyons or drowned river valleys?, *Sedimentary geology*, 58(2-4), 217–235, doi: 10.1016/0037-0738(88)90070-x.
- Ernst, R. E., M. T. D. Wingate, K. L. Buchan, and Z. X. Li (2008), Global record of 1600–700Ma Large Igneous Provinces (LIPs): Implications for the reconstruction of the proposed Nuna (Columbia) and Rodinia supercontinents, *Precambrian research*, 160(1-2), 159–178, doi: 10.1016/j.precamres.2007.04.019.
- Eyster, A., B. P. Weiss, K. Karlstrom, and F. A. Macdonald (2020), Paleomagnetism of the Chuar Group and evaluation of the late Tonian Laurentian apparent polar wander path with implications for the makeup and breakup of Rodinia, *Geological Society of America bulletin*, 132(3-4), 710–738, doi: 10.1130/b32012.1.
- Fabris, A. J., S. A. Constable, A. Woodhouse, S. B. Hore, and M. Fanning (2005), Age, origin, emplacement and mineral potential of the Oodla Wirra Volcanics, Nackara Arc, central Flinders Ranges, South Australia, *Tech. rep.*, Geological Survey of South Australia, Adelaide, South Australia.
- Fanning, C. M. (2007), *A geochronological framework for the gawler craton, south Australia*, Bulletin, Geological Survey of South Australia, Eastwood, NSW, Australia.
- Fanning, C. M., K. R. Ludwig, B. G. Forbes, and W. V. Preiss (1986), Single and multiple grain U–Pb zircon analyses for the early Adelaidean Rook Tuff, Willouran Ranges, South Australia, in *Geological Society of Australia Abstracts, Abstracts*, vol. 15, pp. 71–72, Geological Society of Australia, Sydney, New South Wales.
- Fioretti, A. M., L. P. Black, J. Foden, and D. Visonà (2005), Grenville-age magmatism at the South Tasman Rise (Australia): A new piercing point for the reconstruction of Rodinia, *Geology*, 33(10), 769–772, doi: 10.1130/G21671.1.
- Fitzherbert, J. A., and P. M. Downes (2015), A concise geological history of the Broken Hill region, *Quarterly Notes - Geological Survey of New South Wales*, 143(2), 29–43.
- Fitzsimons, I. C. W. (2000), Grenville-age basement provinces in East Antarctica: Evidence for three separate collisional orogens, *Geology*, 28(10), 879–882, doi: 10.1130/0091-7613(2000)28<879:GBPIEA>2.0.CO;2.
- Flint, R. B., C. M. Fanning, and L. R. Rankin (1988), The Late Proterozoic Kilroo Formation of the Poldia Basin, *South Australia. Geological Survey. Quarterly Geological Notes*, 106, 16–23.
- Foden, J., M. A. Elburg, J. Dougherty-Page, and A. Burt (2006), The timing and duration of the delamerian orogeny: Correlation with the Ross orogen and implications for Gondwana assembly, *The journal of geology*, 114(2), 189–210, doi: 10.1086/499570.
- Foden, J., M. Elburg, S. Turner, C. Clark, M. L. Blades, G. Cox, A. S. Collins, K. Wolff, and C. George (2020), Cambro-Ordovician magmatism in the Delamerian orogeny: Implications for tectonic development of the southern Gondwanan margin, *Gondwana research: international geoscience journal*, 81, 490–521, doi: 10.1016/j.gr.2019.12.006.
- Fraser, G., S. McAvaney, N. Neumann, M. Szpunar, and A. Reid (2010), Discovery of early Mesoarchean crust in the eastern Gawler Craton, South Australia, *Precambrian research*, 179(1-4), 1–21, doi: 10.1016/j.precamres.2010.02.008.
- Fraser, G. L., and N. L. Neumann (2010), New SHRIMP U-Pb Zircon Ages from the Gawler Craton and Curnamona Province, South Australia, 2008 - 2010, *Tech. rep.*, Geoscience Australia, Canberra.
- Gain, S. E. M., Y. Gréau, H. Henry, E. Belousova, I. Dainis, W. L. Griffin, and S. Y. O'Reilly (2019), Mud Tank zircon: Long-term evaluation of a reference material for U-Pb dating, Hf-isotope analysis and trace element analysis, *Geostandards and geoanalytical research*, 43(3), 339–354, doi: 10.1111/ggr.12265.
- Gehling, J. G. (1982), The sedimentology and stratigraphy of the late Precambrian Pound subgroup, Central Flinders Ranges, South Australia, Master's thesis, The University of Adelaide, Adelaide, South Australia.
- Gehling, J. G. (2000), Environmental interpretation and a sequence stratigraphic framework for the terminal Proterozoic Ediacara Member within the Rawnsley Quartzite, South Australia, *Precambrian research*, 100(1-3), 65–95, doi: 10.1016/s0301-9268(99)00069-8.
- Gehling, J. G., and M. L. Droser (2012), Ediacaran stratigraphy and the biota of the Adelaide Geosyncline, South Australia, *Episodes*, 35(1), 236–246, doi: 10.18814/epiiugs/2012/v35i1/023.
- Giddings, J. A., M. W. Wallace, P. W. Haines, and K. Mornane (2010), Submarine origin for the Neoproterozoic Wonoka canyons, South Australia, *Sedimentary geology*, 223(1-2), 35–50, doi: 10.1016/j.sedgeo.2009.10.001.
- Goodge, J. W. (2020), Geological and tectonic evolution of the Transantarctic Mountains, from ancient craton to recent enigma, *Gondwana research: international geoscience journal*, 80, 50–122, doi: 10.1016/j.gr.2019.11.001.
- Goodge, J. W., J. D. Vervoort, C. M. Fanning, D. M. Brecke, G. L. Farmer, I. S. Williams, P. M. Myrow, and D. J. DePaolo (2008), A positive test of East Antarctica-Laurentia juxtaposition within the Rodinia supercontinent, *Science (New York, N.Y.)*, 321(5886), 235–240, doi: 10.1126/science.1159189.
- Goodge, J. W., C. M. Fanning, C. M. Fisher, and J. D. Vervoort (2017), Proterozoic crustal evolution of central East Antarctica: Age and isotopic evidence from glacial igneous clasts, and links with Australia

- and Laurentia, *Precambrian research*, 299, 151–176, doi: 10.1016/j.precamres.2017.07.026.
- Gostin, V. A., P. W. Haines, R. J. Jenkins, W. Compston, and I. S. Williams (1986), Impact ejecta horizon within late precambrian shales, adelaide geosyncline, South Australia, *Science (New York, N.Y.)*, 233(4760), 198–200, doi: 10.1126/science.233.4760.198.
- Gostin, V. A., R. R. Keays, and M. W. Wallace (1989), Iridium anomaly from the Acraman impact ejecta horizon: impacts can produce sedimentary iridium peaks, *Nature*, 340(6234), 542–544, doi: 10.1038/340542a0.
- Grimes, C. B., B. E. John, P. B. Kelemen, F. K. Mazdab, J. L. Wooden, M. J. Cheadle, K. Hanghøj, and J. J. Schwartz (2007), Trace element chemistry of zircons from oceanic crust: A method for distinguishing detrital zircon provenance, *Geology*, 35(7), 643–646, doi: 10.1130/G23603A.1.
- Grimes, C. B., J. L. Wooden, M. J. Cheadle, and B. E. John (2015), “Fingerprinting” tectono-magmatic provenance using trace elements in igneous zircon, *Contributions to mineralogy and petrology. Beitrage zur Mineralogie und Petrologie*, 170(5-6), 46, doi: 10.1007/s00410-015-1199-3.
- Haines, P. W. (1987), Carbonate shelf and basin sedimentation, late Proterozoic Wonoka Formation, South Australia, Ph.D. thesis, The University of Adelaide, Adelaide, South Australia.
- Hall, J. W. (2018), The thermochronological evolution of the northern Gawler Craton and northern Adelaide Rift Complex, Ph.D. thesis, University of Adelaide, Adelaide, Australia.
- Halpin, J. A., T. Jensen, P. McGoldrick, S. Meffre, R. F. Berry, J. L. Everard, C. R. Calver, J. Thompson, K. Goemann, and J. M. Whittaker (2014), Authigenic monazite and detrital zircon dating from the Proterozoic Rocky Cape Group, Tasmania: Links to the Belt-Purcell Supergroup, North America, *Precambrian research*, 250, 50–67, doi: 10.1016/j.precamres.2014.05.025.
- Hoffman, P. F. (1991), Did the breakout of Laurentia turn Gondwanaland inside-out?, *Science (New York, N.Y.)*, 252(5011), 1409–1412, doi: 10.1126/science.252.5011.1409.
- Horstwood, M. S. A., J. Košler, G. Gehrels, S. E. Jackson, N. M. McLean, C. Paton, N. J. Pearson, K. Sircombe, P. Sylvester, P. Vermeesch, J. F. Bowring, D. J. Condon, and B. Schoene (2016), Community-derived standards for LA - ICP - MS U-(Th-)Pb geochronology – uncertainty propagation, age interpretation and data reporting, *Geostandards and geoanalytical research*, 40(3), 311–332, doi: 10.1111/j.1751-908x.2016.00379.x.
- Hoskin, P. W. O. (2003), The composition of zircon and igneous and metamorphic petrogenesis, *Reviews in mineralogy and geochemistry*, 53(1), 27–62, doi: 10.2113/0530027.
- Hoskin, P. W. O., and T. R. Ireland (2000), Rare earth element chemistry of zircon and its use as a provenance indicator, *Geology*, 28(7), 627–630, doi: 10.1130/0091-7613(2000)28<627:REECOZ>2.0.CO;2.
- Howard, H. M., R. H. Smithies, C. L. Kirkland, D. E. Kelsey, A. Aitken, M. T. D. Wingate, R. Quentin de Gromard, C. V. Spaggiari, and W. D. Maier (2015), The burning heart — The Proterozoic geology and geological evolution of the west Musgrave Region, central Australia, *Gondwana research: international geoscience journal*, 27(1), 64–94, doi: 10.1016/j.gr.2014.09.001.
- Howchin, W. (1904), The geology of the Mount Lofty Ranges: Part I, *Transactions of the Royal Society of South Australia, Incorporated. Royal Society of South Australia*, 28, 253–280.
- Hui, B., Y. Dong, F. Zhang, S. Sun, and S. He (2021), Neoproterozoic active margin in the northwestern Yangtze Block, South China: new clues from detrital zircon U–Pb geochronology and geochemistry of sedimentary rocks from the Hengdan Group, *Geological magazine*, 158(5), 842–858, doi: 10.1017/s0016756820000898.
- Ireland, T. R., T. Flöttmann, C. M. Fanning, G. M. Gibson, and W. V. Preiss (1998), Development of the early Paleozoic Pacific margin of Gondwana from detrital-zircon ages across the Delamerian orogen, *Geology*, 26(3), 243–246, doi: 10.1130/0091-7613(1998)026<0243:DOTOPP>2.3.CO;2.
- Jackson, S. E., N. J. Pearson, W. L. Griffin, and E. A. Belousova (2004), The application of laser ablation-inductively coupled plasma-mass spectrometry to in situ U–Pb zircon geochronology, *Chemical geology*, 211(1-2), 47–69, doi: 10.1016/j.chemgeo.2004.06.017.
- Jacobs, J., M. Elburg, A. Läufer, I. C. Kleinhanns, F. Henjes-Kunst, S. Estrada, A. S. Ruppel, D. Damaske, P. Montero, and F. Bea (2015), Two distinct Late Mesoproterozoic/Early Neoproterozoic basement provinces in central/eastern Dronning Maud Land, East Antarctica: The missing link, 15–21°E, *Precambrian research*, 265, 249–272, doi: 10.1016/j.precamres.2015.05.003.
- Jacobs, J., B. Opås, M. A. Elburg, A. Läufer, S. Estrada, A. K. Ksienzyk, D. Damaske, and M. Hofmann (2017), Cryptic sub-ice geology revealed by a U–Pb zircon study of glacial till in Dronning Maud Land, East Antarctica, *Precambrian research*, 294, 1–14, doi: 10.1016/j.precamres.2017.03.012.
- Jago, J. B., J. G. Gehling, M. J. Betts, G. A. Brock, C. R. Dalgarno, D. C. García-Bellido, P. G. Haslett, S. M. Jacquet, P. D. Kruse, N. R. Langsford, T. J. Mount, and J. R. Paterson (2018), The Cambrian system in the arrowie basin, Flinders ranges, south Australia, *Australian journal of earth sciences*, 67(7), 923–948, doi: 10.1080/08120099.2018.1525431.
- Jagodzinski, E. A., and C. E. Fricke (2010), Compilation of new SHRIMP U–Pb geochronological data for the Southern Curnamona Province, South Australia, 2010, *Tech. rep.*, Geological Survey of South Australia, Adelaide, South Australia.
- Jagodzinski, E. A., and S. O. McAvaney (2017), SHRIMP U–Pb geochronology data for northern Eyre Peninsula, 2014–2016, *Tech. Rep. 2016/00001*, Geological Survey of South Australia, Adelaide, Australia, doi: 10.13140/RG.2.2.10517.52960.
- Jagodzinski, E. A., M. Werner, S. Curtis, A. Fabris, M. Pawley, and C. Krapf (2020), SHRIMP Geochronology of the Mt Double area, Southern Gawler Ranges margin, *Tech. rep.*, Geological Survey of South Australia, South Australia.
- Jagodzinski, E. A., A. J. Reid, J. L. Crowley, C. E. Wade, and S. Curtis (2023), Precise zircon U–Pb dating of the Mesoproterozoic Gawler large igneous province, South Australia, *Results in Geochemistry*, 10(100020), 100,020, doi: 10.1016/j.ringeo.2022.100020.
- Job, A. L. (2011), Evolution of the basal Adelaidean in the northern Flinders Ranges: deposition, provenance and deformation of the Callanna and lower Burra Groups,

- Ph.D. thesis, The University of Adelaide, Adelaide, South Australia.
- Jochum, K. P., U. Weis, B. Stoll, D. Kuzmin, Q. Yang, I. Raczek, D. E. Jacob, A. Stracke, K. Birbaum, D. A. Frick, D. Günther, and J. Enzweiler (2011), Determination of Reference Values for NIST SRM 610–617 Glasses Following ISO Guidelines, *Geostandards and geoanalytical research*, 35(4), 397–429, doi: 10.1111/j.1751-908X.2011.00120.x.
- Johansson, A., B. Bingen, H. Huhma, T. Waight, R. Vestergaard, A. Soesoo, G. Skridlaite, E. Krzeminska, L. Shumlyansky, M. E. Holland, C. Holm-Denoma, W. Teixeira, F. M. Faleiros, B. V. Ribeiro, J. Jacobs, C. Wang, R. J. Thomas, P. H. Macey, C. L. Kirkland, M. I. H. Hartnady, B. M. Eglington, S. J. Puetz, and K. C. Condie (2022), A geochronological review of magmatism along the external margin of Columbia and in the Grenville-age orogens forming the core of Rodinia, *Precambrian research*, 371(106463), 106,463, doi: 10.1016/j.precamres.2021.106463.
- Karlstrom, K. (1999), Refining Rodinia: Geologic Evidence for the Australia–Western U.S. connection in the Proterozoic, *GSA today: a publication of the Geological Society of America*, 9(10), 1–7, doi: 10.1130/gsat-1999-10-01-science.
- Karlstrom, K. E., and S. A. Bowring (1988), Early Proterozoic assembly of tectonostratigraphic terranes in southwestern north America, *The journal of geology*, 96(5), 561–576, doi: 10.1086/629252.
- Keeman, J., S. Turner, P. W. Haines, E. Belousova, T. Ireland, P. Brouwer, J. Foden, and G. Wörner (2020), New U Pb, Hf and O isotope constraints on the provenance of sediments from the Adelaide Rift Complex – Documenting the key Neoproterozoic to early Cambrian succession, *Gondwana research: international geoscience journal*, 83, 248–278, doi: 10.1016/j.gr.2020.02.005.
- Kendall, B. S., R. A. Creaser, and D. Selby (2006), Re-Os geochronology of postglacial black shales in Australia: Constraints on the timing of “Sturtian” glaciation, *Geology*, 34(9), 729–732, doi: 10.1130/G22775.1.
- Lan, Z., X.-H. Li, M. Zhu, Q. Zhang, and Q.-L. Li (2015), Revisiting the Liantuo Formation in Yangtze Block, South China: SIMS U–Pb zircon age constraints and regional and global significance, *Precambrian research*, 263, 123–141, doi: 10.1016/j.precamres.2015.03.012.
- Le Heron, D. P. (2012), The Cryogenian record of glaciation and deglaciation in South Australia, *Sedimentary geology*, 243–244, 57–69, doi: 10.1016/j.sedgeo.2011.09.013.
- Le Heron, D. P., G. Cox, A. Trundle, and A. S. Collins (2011), Two Cryogenian glacial successions compared: Aspects of the Sturt and Elatina sediment records of South Australia, *Precambrian research*, 186(1–4), 147–168, doi: 10.1016/j.precamres.2011.01.014.
- Lechte, M. A., and M. W. Wallace (2015), Sedimentary and tectonic history of the Holowilena Ironstone, a Neoproterozoic iron formation in South Australia, *Sedimentary geology*, 329, 211–224, doi: 10.1016/j.sedgeo.2015.09.014.
- Li, Z.-X., L. Zhang, and C. M. Powell (1995), South China in Rodinia: Part of the missing link between Australia–East Antarctica and Laurentia?, *Geology*, 23(5), 407–410, doi: 10.1130/0091-7613(1995)023<0407:SCIRPO>2.3.CO;2.
- Li, Z. X., S. V. Bogdanova, A. S. Collins, A. Davidson, B. De Waele, R. E. Ernst, I. C. W. Fitzsimons, R. A. Fuck, D. P. Gladkochub, J. Jacobs, K. E. Karlstrom, S. Lu, L. M. Natapov, V. Pease, S. A. Pisarevsky, K. Thrane, and V. Vernikovsky (2008), Assembly, configuration, and break-up history of Rodinia: A synthesis, *Precambrian research*, 160(1–2), 179–210, doi: 10.1016/j.precamres.2007.04.021.
- Lindsay, C. C. (1973), The Stratigraphy and Sedimentology of the Mount Saturday Area, Northern Flinders Ranges, South Australia, Ph.D. thesis, Adelaide University, Adelaide, South Australia.
- Lloyd, J. C., M. L. Blades, J. W. Counts, A. S. Collins, K. J. Amos, B. P. Wade, J. W. Hall, S. Hore, A. L. Ball, S. Shahin, and M. Drabsch (2020), Neoproterozoic geochronology and provenance of the Adelaide Superbasin, *Precambrian research*, 350(105849), 105,849, doi: 10.1016/j.precamres.2020.105849.
- Lloyd, J. C., A. S. Collins, M. L. Blades, S. E. Gilbert, and K. J. Amos (2022), Early evolution of the Adelaide Superbasin, *Geosciences*, 12(4), 154, doi: 10.3390/geosciences12040154.
- Lloyd, J. C., W. V. Preiss, A. S. Collins, G. M. Virgo, M. L. Blades, S. E. Gilbert, D. Subarkah, C. B. E. Krapf, and K. J. Amos (2023), Geochronology and formal stratigraphy of the Sturtian Glaciation in the Adelaide Superbasin, *Geological magazine*, 160(7), 1321–1344, doi: 10.1017/s0016756823000390.
- Lubiniecki, D. C., R. C. King, S. P. Holford, M. A. Bunch, S. B. Hore, and S. M. Hill (2020), Cenozoic structural evolution of the Mount Lofty Ranges and Flinders Ranges, South Australia, constrained by analysis of deformation bands, *Australian journal of earth sciences*, 67(8), 1097–1115, doi: 10.1080/08120099.2019.1695227.
- Mackay, W. G. (2011), Structure and sedimentology of the Curdimurka subgroup, northern Adelaide Fold Belt, South Australia, Ph.D. thesis, University of Tasmania, Hobart, Tasmania, doi: 10.25959/23210435.V1.
- MacLennan, S. A., M. P. Eddy, A. J. Merschat, A. K. Mehra, P. W. Crockford, A. C. Maloof, C. S. Southworth, and B. Schoene (2020), Geologic evidence for an icehouse Earth before the Sturtian global glaciation, *Science advances*, 6(24), eaay6647, doi: 10.1126/sciadv.aay6647.
- Mancktelow, N. S. (1979), The structure and metamorphism of the southern Adelaide Fold Belt, Ph.D. thesis, The University of Adelaide, Adelaide, South Australia.
- Matenco, L. C., and B. U. Haq (2020), Multi-scale depositional successions in tectonic settings, *Earth-science reviews*, 200(102991), 102,991, doi: 10.1016/j.earscirev.2019.102991.
- Mawson, D. (1947), The Adelaide Series as developed along the western margin of the Flinders Ranges, *Transactions of the Royal Society of South Australia, Incorporated. Royal Society of South Australia*, 71, 259–280.
- Mawson, D., and R. C. Sprigg (1950), Subdivision of the Adelaide System, *The Australian journal of science*, 13(3), 69–72.
- McAvaney, S. (2012), The Cooyerdoo Granite: Paleo- and Mesoarchean basement of the Gawler Craton, *MESA Journal*, 90(15), 80.
- McAvaney, S. O., M. Werner, M. J. Pawley, C. B. E. Krapf, and B. E. Nicolson (2016), Geology of the Six Mile Hill 1:75 000 Map Sheet, Mineral Systems Drilling Program Special Map Series, *Tech. rep.*, Geological Survey of South Australia, Adelaide, South Australia.
- Meaney, K. J. (2012), The geochronology and structural evolution of the Warren Inlier and Springfield Sequence,

- Mt. Lofty Ranges: Implications for Proterozoic paleogeographic reconstructions, Ph.D. thesis, The University of Adelaide, Adelaide, South Australia.
- Meaney, K. J. (2017), Proterozoic crustal growth in the southeastern Gawler Craton: The development of the Barossa Complex, and an assessment of the detrital zircon method, Ph.D. thesis, The University of Adelaide, Adelaide, South Australia.
- Merdith, A. S., A. S. Collins, S. E. Williams, S. Pisarevsky, J. D. Foden, D. B. Archibald, M. L. Blades, B. L. Alessio, S. Armistead, D. Plavsa, C. Clark, and R. D. Müller (2017), A full-plate global reconstruction of the Neoproterozoic, *Gondwana research: international geoscience journal*, 50, 84–134, doi: 10.1016/j.gr.2017.04.001.
- Merdith, A. S., S. E. Williams, S. Brune, A. S. Collins, and R. D. Müller (2019), Rift and plate boundary evolution across two supercontinent cycles, *Global and planetary change*, 173, 1–14, doi: 10.1016/j.gloplacha.2018.11.006.
- Merdith, A. S., S. E. Williams, A. S. Collins, M. G. Tetley, J. A. Mulder, M. L. Blades, A. Young, S. E. Armistead, J. Cannon, S. Zahirovic, and R. D. Müller (2021), Extending full-plate tectonic models into deep time: Linking the Neoproterozoic and the Phanerozoic, *Earth-science reviews*, 214(103477), 103,477, doi: 10.1016/j.earscirev.2020.103477.
- Moores, E. M. (1991), Southwest U.S.-East Antarctic (SWEAT) connection: A hypothesis, *Geology*, 19(5), 425–428, doi: 10.1130/0091-7613(1991)019<0425:SUSEAS>2.3.CO;2.
- Morrissey, L. J., K. M. Barovich, M. Hand, K. E. Howard, and J. L. Payne (2019), Magmatism and metamorphism at ca. 1.45 Ga in the northern Gawler Craton: The Australian record of rifting within Nuna (Columbia), *Geoscience frontiers*, 10(1), 175–194, doi: 10.1016/j.gsf.2018.07.006.
- Mount, T. J. (1976), Diapirs and diapirism in the Adelaide 'Geosyncline', South Australia, Ph.D. thesis, The University of Adelaide, Adelaide, South Australia.
- Mulder, J. A., J. A. Halpin, and N. R. Daczko (2015), Mesoproterozoic Tasmania: Witness to the East Antarctica-Laurentia connection within Nuna, *Geology*, 43(9), 759–762, doi: 10.1130/G36850.1.
- Mulder, J. A., K. E. Karlstrom, J. A. Halpin, A. S. Merdith, C. J. Spencer, R. F. Berry, and B. McDonald (2018a), Rodinian devil in disguise: Correlation of 1.25–1.10 Ga strata between Tasmania and Grand Canyon, *Geology*, 46(11), 991–994, doi: 10.1130/G45225.1.
- Mulder, J. A., R. F. Berry, J. A. Halpin, S. Meffre, and J. L. Everard (2018b), Depositional age and correlation of the Oonah Formation: refining the timing of Neoproterozoic basin formation in Tasmania, *Australian journal of earth sciences*, 65(3), 391–407, doi: 10.1080/08120099.2018.1426629.
- Mulder, J. A., J. L. Everard, G. Cumming, S. Meffre, R. S. Bottrill, A. S. Merdith, J. A. Halpin, A. W. McNeill, and P. A. Cawood (2020), Neoproterozoic opening of the Pacific Ocean recorded by multi-stage rifting in Tasmania, Australia, *Earth-science reviews*, 201(103041), 103,041, doi: 10.1016/j.earscirev.2019.103041.
- Murrell, B. (1977), Stratigraphy and tectonics across the Torrens hinge zone between Andamooka and Marree, South Australia [microform], Ph.D. thesis, Adelaide,, Adelaide, South Australia.
- Norris, A., and L. Danyushevsky (2018), Towards estimating the complete uncertainty budget of quantified results measured by LA-ICP-MS, *Goldschmidt: Boston, MA, USA*.
- O'Neill, H. S. C. (2016), The smoothness and shapes of chondrite-normalized rare earth element patterns in basalts, *Journal of petrology*, 57(8), 1463–1508, doi: 10.1093/petrology/egw047.
- Page, R. W., B. P. J. Stevens, and G. M. Gibson (2005), Geochronology of the sequence hosting the Broken Hill Pb-Zn-Ag orebody, Australia, *Economic geology and the bulletin of the Society of Economic Geologists*, 100(4), 633–661, doi: 10.2113/gsecongeo.100.4.633.
- Park, Y., N. L. Swanson-Hysell, H. Xian, S. Zhang, D. J. Condon, H. Fu, and F. A. Macdonald (2021), A consistently high-latitude South China from 820 to 780 ma: Implications for exclusion from Rodinia and the feasibility of large-scale true polar wander, *Journal of geophysical research. Solid earth*, 126(6), doi: 10.1029/2020jb021541.
- Powell, C. M., W. V. Preiss, C. G. Gatehouse, B. Krapez, and Z. X. Li (1994), South Australian record of a Rodinian epicontinental basin and its mid-neoproterozoic breakup (1700 Ma) to form the Palaeo-Pacific Ocean, *Tectonophysics*, 237(3-4), 113–140, doi: 10.1016/0040-1951(94)90250-x.
- Preiss, W., C. Fanning, M. Szpunar, and A. Burt (2008), Age and tectonic significance of the Mount Crawford Granite Gneiss and a related intrusive in the Oakbank Inlier, Mount Lofty Ranges, South Australia, *MESA Journal*, 49, 38–49.
- Preiss, W. V. (1987), *Adelaide Geosyncline-late Proterozoic stratigraphy, sedimentation, palaeontology and tectonics*, Bulletin, Geological Survey of South Australia, Eastwood, NSW, Australia.
- Preiss, W. V. (1993), Neoproterozoic, in *The geology of South Australia, Bulletin*, vol. 1 The Precambrian, edited by J. F. Drexel, W. V. Preiss, and A. J. Parker, pp. 171–204, Geological Survey of South Australia, South Australia.
- Preiss, W. V. (1997), Revision of lithostratigraphy and structure, and evidence of volcanism in Lower Burra Group type sections, Carey Gully-Basket Range Area, Mount Lofty Ranges, *MESA Journal*, 7, 37–46.
- Preiss, W. V. (2000), The Adelaide Geosyncline of South Australia and its significance in Neoproterozoic continental reconstruction, *Precambrian research*, 100(1-3), 21–63, doi: 10.1016/s0301-9268(99)00068-6.
- Preiss, W. V., and W. M. Cowley (1999), Genetic stratigraphy and revised lithostratigraphic classification of the Burra Group in the Adelaide Geosyncline, *MESA Journal*, 14, 30–40.
- Preiss, W. V., I. A. Dyson, P. W. Reid, and W. M. Cowley (1998), Revision of lithostratigraphic classification of the Umberatana Group, *MESA Journal*, 9, 36–42.
- Preiss, W. V., J. F. Drexel, and A. J. Reid (2009), Definition and age of the Koorunga Member of the Skillogalee Dolomite: host for Neoproterozoic (c. 790 Ma) porphyry-related copper mineralisation at Burra, *MESA Journal*, 55, 19–33.
- Reid, A. J., and M. Hand (2012), Mesoarchean to Mesoproterozoic evolution of the southern Gawler Craton, South Australia, *Episodes*, 35(1), 216–225, doi: 10.18814/epiugs/2012/v35i1/021.
- Reid, A. J., and E. A. Jagodzinski (2011), *PACE Geochronology: Results of collaborative geochronology projects 2009-2010*, Report Book, Geological Survey of South Australia, Eastwood, NSW, Australia.
- Reid, A. J., and J. L. Payne (2017), Magmatic zircon Lu-Hf isotopic record of juvenile addition and crustal reworking

- in the Gawler Craton, Australia, *Lithos*, 292-293, 294–306, doi: 10.1016/j.lithos.2017.08.010.
- Reid, A. J., E. A. Jagodzinski, G. L. Fraser, and M. J. Pawley (2014), SHRIMP U–Pb zircon age constraints on the tectonics of the Neoproterozoic to early Paleoproterozoic transition within the Mulgathing Complex, Gawler Craton, South Australia, *Precambrian research*, 250, 27–49, doi: 10.1016/j.precamres.2014.05.013.
- Reid, A. J., J. A. Halpin, and R. A. Dutch (2019), Timing and style of high-temperature metamorphism across the Western Gawler Craton during the Paleo- to Mesoproterozoic, *Australian journal of earth sciences*, 66(8), 1085–1111, doi: 10.1080/08120099.2019.1602565.
- Retallack, G. J., A. Marconato, J. T. Osterhout, K. E. Watts, and I. N. Bindeman (2014), Revised Wonoka isotopic anomaly in South Australia and Late Ediacaran mass extinction, *Journal of the Geological Society*, 171(5), 709–722, doi: 10.1144/jgs2014-016.
- Rooney, A. D., J. V. Strauss, A. D. Brandon, and F. A. Macdonald (2015), A Cryogenian chronology: Two long-lasting synchronous Neoproterozoic glaciations, *Geology*, 43(5), 459–462, doi: 10.1130/G36511.1.
- Rose, C. V., A. C. Maloof, B. Schoene, R. C. Ewing, U. Linnemann, M. Hofmann, and J. M. Cottle (2013), The end-Cryogenian glaciation of South Australia, *Geoscience Canada*, 40(4), 256, doi: 10.12789/geocanj.2013.40.019.
- Rowan, M. G., T. E. Hearon, IV, R. A. Kernen, K. A. Giles, C. E. Gannaway-Dalton, N. J. Williams, J. C. Fiduk, T. F. Lawton, P. T. Hannah, and M. P. Fischer (2020), A review of allochthonous salt tectonics in the Flinders and Willouran ranges, South Australia, *Australian journal of earth sciences*, 67(6), 787–813, doi: 10.1080/08120099.2018.1553063.
- Rubatto, D. (2002), Zircon trace element geochemistry: partitioning with garnet and the link between U–Pb ages and metamorphism, *Chemical geology*, 184(1-2), 123–138, doi: 10.1016/s0009-2541(01)00355-2.
- Shahin, S. (2016), Structural analysis and facies distribution of Cryogenian glacial rocks and regional structures in the Willouran Ranges, SA, Ph.D. thesis, The University of Adelaide, Adelaide, South Australia.
- Shannon, R. D. (1976), Revised effective ionic radii and systematic studies of interatomic distances in halides and chalcogenides, *Acta crystallographica. Section A, Crystal physics, diffraction, theoretical and general crystallography*, 32(5), 751–767, doi: 10.1107/S0567739476001551.
- Sheard, M. J. (2012), MARREE, *Tech. rep.*, Geological Survey of South Australia, Adelaide, South Australia.
- Sheibner, E., and H. Basden (1998), *Geology of New South Wales - Synthesis, Geology Memoir*, vol. 13(2), Department of Mineral Resources, Sydney, New South Wales.
- Shu, L., J. Yao, B. Wang, M. Faure, J. Charvet, and Y. Chen (2021), Neoproterozoic plate tectonic process and Phanerozoic geodynamic evolution of the South China Block, *Earth-science reviews*, 216(103596), 103,596, doi: 10.1016/j.earscirev.2021.103596.
- Sláma, J., and J. Košler (2012), Effects of sampling and mineral separation on accuracy of detrital zircon studies, *Geochemistry, geophysics, geosystems: G(3)*, 13(5), doi: 10.1029/2012GC004106.
- Sláma, J., J. Košler, D. J. Condon, J. L. Crowley, A. Gerdes, J. M. Hanchar, M. S. A. Horstwood, G. A. Morris, L. Nasdala, N. Norberg, U. Schaltegger, B. Schoene, M. N. Tubrett, and M. J. Whitehouse (2008), Plešovice zircon — A new natural reference material for U–Pb and Hf isotopic microanalysis, *Chemical geology*, 249(1-2), 1–35, doi: 10.1016/j.chemgeo.2007.11.005.
- Smithies, R. H., H. M. Howard, P. M. Evins, C. L. Kirkland, S. Bodorkos, and M. T. D. Wingate (2008), The west Musgrave Complex - new geological insights from recent mapping, geochronology, and geochemical studies, *Tech. rep.*, Geological Survey of Western Australia.
- Smithies, R. H., H. M. Howard, P. M. Evins, C. L. Kirkland, D. E. Kelsey, M. Hand, M. T. D. Wingate, A. S. Collins, and E. Belousova (2011), High-temperature granite magmatism, crust–mantle interaction and the mesoproterozoic intracontinental evolution of the Musgrave province, central Australia, *Journal of petrology*, 52(5), 931–958, doi: 10.1093/petrology/egr010.
- Smits, R. G., W. J. Collins, M. Hand, R. Dutch, and J. Payne (2014), A Proterozoic Wilson cycle identified by Hf isotopes in central Australia: Implications for the assembly of Proterozoic Australia and Rodinia, *Geology*, 42(3), 231–234, doi: 10.1130/G35112.1.
- Spaggiari, C. V., C. L. Kirkland, R. H. Smithies, M. T. D. Wingate, and E. A. Belousova (2015), Transformation of an Archean craton margin during Proterozoic basin formation and magmatism: The Albany–Fraser Orogen, Western Australia, *Precambrian research*, 266, 440–466, doi: 10.1016/j.precamres.2015.05.036.
- Spencer, C. J., C. L. Kirkland, and R. J. M. Taylor (2016), Strategies towards statistically robust interpretations of in situ U–Pb zircon geochronology, *Geoscience frontiers*, 7(4), 581–589, doi: 10.1016/j.gsf.2015.11.006.
- Sprigg, R. C. (1952), Sedimentation in the Adelaide Geosyncline and the formation of the continental terrace, *Sir Douglas Mawson anniversary volume*, pp. 153–159.
- Squire, R., I. Campbell, C. Allen, and C. Wilson (2006), Did the Transgondwanan Supermountain trigger the explosive radiation of animals on Earth?, *Earth and planetary science letters*, 250(1-2), 116–133, doi: 10.1016/j.epsl.2006.07.032.
- Strauss, J. V., F. A. Macdonald, G. P. Halverson, N. J. Tosca, D. P. Schrag, and A. H. Knoll (2015), Stratigraphic evolution of the Neoproterozoic Callison Lake Formation: Linking the break-up of Rodinia to the Islay carbon isotope excursion, *American journal of science*, 315(10), 881–944, doi: 10.2475/10.2015.01.
- Stüeken, E. E., R. Buick, and T. W. Lyons (2019), Revisiting the depositional environment of the Neoproterozoic Callanna Group, South Australia, *Precambrian research*, 334(105474), 105,474, doi: 10.1016/j.precamres.2019.105474.
- Swain, G., A. Woodhouse, M. Hand, K. Barovich, M. Schwarz, and C. M. Fanning (2005), Provenance and tectonic development of the late Archaean Gawler Craton, Australia; U–Pb zircon, geochemical and Sm–Nd isotopic implications, *Precambrian research*, 141(3-4), 106–136, doi: 10.1016/j.precamres.2005.08.004.
- Tang, Q., Z. Zhang, C. Li, Y. Wang, and E. M. Ripley (2016), Neoproterozoic subduction-related basaltic magmatism in the northern margin of the Tarim Craton: Implications for Rodinia reconstruction, *Precambrian research*, 286, 370–378, doi: 10.1016/j.precamres.2016.10.012.
- Tonkin, D., and C. Wallace (2021), Stratigraphy, diagenesis and copper sulfide mineralisation in the

- Whyalla Sandstone, Stuart Shelf, and implications for stratabound mineral exploration, *MESA Journal*, 94(1), 23–40.
- Toteff, S. (1977), The geology of the Adelaidean-Kanmantoo group sequences in the eastern Mount Lofty Ranges, Ph.D. thesis, The University of Adelaide, Adelaide.
- Turnbull, R. E., J. J. Schwartz, M. L. Fiorentini, R. Jongens, N. J. Evans, T. Ludwig, B. J. McDonald, and K. A. Klepeis (2021), A hidden Rodinian lithospheric keel beneath Zealandia, Earth's newly recognized continent, *Geology*, 49(8), 1009–1014, doi: 10.1130/g48711.1.
- Uppil, R. K. (1980), Sedimentology of the late Precambrian Mundallio Subgroup : a clastic-carbonate (Dolomite, Magnesite) sequence in the Mt. Lofty and Flinders Ranges, South Australia, Ph.D. thesis, The University of Adelaide, Adelaide, South Australia.
- Urlwin, B. (1992), Carbon isotope stratigraphy of the Late Proterozoic Wonoka Formation of the Adelaide Fold Belt: diagenetic assessment and interpretation of isotopic signature and correlations with previously measured isotopic curves, Ph.D. thesis, The University of Adelaide, Adelaide, South Australia.
- Van der Wolff, E. J. (2020), Detrital provenance and geochronology of the Burra, Umberatana and Wilpena groups in the Mount Lofty Ranges, Ph.D. thesis, The University of Adelaide, Adelaide, South Australia.
- Verdel, C., M. J. Campbell, and C. M. Allen (2021), Detrital zircon petrochronology of central Australia, and implications for the secular record of zircon trace element composition, *Geosphere*, 17(2), 538–560, doi: 10.1130/ges02300.1.
- Vermeesch, P. (2018), IsoplotR: A free and open toolbox for geochronology, *Geoscience frontiers*, 9(5), 1479–1493, doi: 10.1016/j.gsf.2018.04.001.
- Vermeesch, P., A. Resentini, and E. Garzanti (2016), An R package for statistical provenance analysis, *Sedimentary geology*, 336, 14–25, doi: 10.1016/j.sedgeo.2016.01.009.
- Virgo, G. M., A. S. Collins, K. J. Amos, J. Farkaš, M. L. Blades, and D. Subarkah (2021), Descending into the “snowball”: High resolution sedimentological and geochemical analysis across the Tonian to Cryogenian boundary in South Australia, *Precambrian research*, 367(106449), 106,449, doi: 10.1016/j.precamres.2021.106449.
- Virgo, G. M., A. S. Collins, M. L. Blades, and K. J. Amos (2023), Tectonic, eustatic and climate controls on facies architecture during the transition to the Neoproterozoic icehouse in the Adelaide Superbasin, Australia, *Sedimentologica*, 1(1), 1–38, doi: 10.57035/journals/sdk.2023.e11.1083.
- Wade, B. P., D. E. Kelsey, M. Hand, and K. M. Barovich (2008), The Musgrave Province: Stitching north, west and south Australia, *Precambrian research*, 166(1-4), 370–386, doi: 10.1016/j.precamres.2007.05.007.
- Wade, C. E. (2011), Definition of the Mesoproterozoic Ninnerie Supersuite, Curnamona Province, South Australia, *MESA Journal*, 62, 25–42.
- Wen, B., D. A. D. Evans, and Y.-X. Li (2017), Neoproterozoic paleogeography of the Tarim Block: An extended or alternative “missing-link” model for Rodinia?, *Earth and planetary science letters*, 458, 92–106, doi: 10.1016/j.epsl.2016.10.030.
- Wen, B., D. A. D. Evans, C. Wang, Y.-X. Li, and X. Jing (2018), A positive test for the Greater Tarim Block at the heart of Rodinia: Mega-dextral suturing of supercontinent assembly, *Geology*, 46(8), 687–690, doi: 10.1130/g40254.1.
- Wiedenbeck, M., P. Allé, F. Corfu, W. L. Griffin, M. Meier, F. Oberli, A. V. O. N. Quadt, J. C. Roddick, and W. Spiegel (1995), Three natural zircon standards for u-Th-Pb, Lu-Hf, trace element and Re analyses, *Geostandards newsletter*, 19(1), 1–23, doi: 10.1111/j.1751-908x.1995.tb00147.x.
- Wiedenbeck, M., J. M. Hanchar, W. H. Peck, P. Sylvester, J. Valley, M. Whitehouse, A. Kronz, Y. Morishita, L. Nasdala, J. Fiebig, I. Franchi, J. P. Girard, R. C. Greenwood, R. Hinton, N. Kita, P. R. D. Mason, M. Norman, M. Ogasawara, P. M. Piccoli, D. Rhede, H. Satoh, B. Schulz-Dobrick, O. Skår, M. J. Spicuzza, K. Terada, A. Tindle, S. Togashi, T. Vennemann, Q. Xie, and Y. F. Zheng (2004), Further Characterisation of the 91500 Zircon Crystal, *Geostandards and geoanalytical research*, 28(1), 9–39, doi: 10.1111/j.1751-908x.2004.tb01041.x.
- Williams, G. E., and P. W. Schmidt (2018), Shuram–Wonoka carbon isotope excursion: Ediacaran revolution in the world ocean's meridional overturning circulation, *Geoscience frontiers*, 9(2), 391–402, doi: 10.1016/j.gsf.2017.11.006.
- Williams, G. E., and D. G. Tonkin (1985), Periglacial structures and palaeoclimatic significance of a late Precambrian block field in the Cattle Grid copper mine, Mount Gunson, South Australia, *Australian journal of earth sciences*, 32(3), 287–300, doi: 10.1080/08120098508729331.
- Williams, G. E., V. A. Gostin, D. M. McKirdy, and W. V. Preiss (2008), The Elatina glaciation, late Cryogenian (Marinoan Epoch), South Australia: Sedimentary facies and palaeoenvironments, *Precambrian research*, 163(3-4), 307–331, doi: 10.1016/j.precamres.2007.12.001.
- Williams, M. A., and A. J. Reid (2021), Linking lithostratigraphy to mineral potential for the Archean to earliest Paleoproterozoic Mulgathing Complex, central Gawler Craton, *MESA Journal*, 94, 4–18.
- Williams, M. A., D. E. Kelsey, M. Hand, T. Raimondo, L. J. Morrissey, N. M. Tucker, and R. A. Dutch (2018), Further evidence for two metamorphic events in the Mawson Continent, *Antarctic science*, 30(1), 44–65, doi: 10.1017/s0954102017000451.
- Wingate, M. T. D., and J. W. Giddings (2000), Age and palaeomagnetism of the Mundine Well dyke swarm, Western Australia: implications for an Australia–Laurentia connection at 755 Ma, *Precambrian research*, 100(1-3), 335–357, doi: 10.1016/s0301-9268(99)00080-7.
- Wingate, M. T. D., I. H. Campbell, W. Compston, and G. M. Gibson (1998), Ion microprobe U–Pb ages for Neoproterozoic basaltic magmatism in south-central Australia and implications for the breakup of Rodinia, *Precambrian research*, 87(3-4), 135–159, doi: 10.1016/s0301-9268(97)00072-7.
- Wingate, M. T. D., S. A. Pisarevsky, and D. A. D. Evans (2002), Rodinia connections between Australia and Laurentia: no SWEAT, no AUSWUS?: Rodinia connections between Australia and Laurentia, *Terra nova*, 14(2), 121–128, doi: 10.1046/j.1365-3121.2002.00401.x.
- Wu, G., Y. Xiao, B. Bonin, D. Ma, X. Li, and G. Zhu (2018), Ca. 850 Ma magmatic events in the Tarim Craton: Age, geochemistry and implications for assembly of Rodinia supercontinent, *Precambrian research*, 305, 489–503, doi: 10.1016/j.precamres.2017.10.020.

- Wu, G., S. Yang, W. Liu, R. D. Nance, X. Chen, Z. Wang, and Y. Xiao (2021), Switching from advancing to retreating subduction in the Neoproterozoic Tarim Craton, NW China: Implications for Rodinia breakup, *Geoscience frontiers*, 12(1), 161–171, doi: 10.1016/j.gsf.2020.03.013.
- Young, G. M., and V. A. Gostin (1991), Late Proterozoic (Sturtian) succession of the North Flinders Basin, South Australia; An example of temperate glaciation in an active rift setting, in *Geological Society of America Special Papers, Geological Society of America Special Papers*, vol. 261, edited by J. B. Anderson and G. M. Ashley, pp. 207–222, Geological Society of America, doi: 10.1130/spe261-p207.
- Young, T. (1995), The Bunyeroo Formation and its possible cold-water marine setting, Ph.D. thesis, University of Adelaide, Department of Geology and Geophysics, Adelaide, South Australia.
- Zhang, C.-L., H.-B. Zou, Q.-B. Zhu, and X.-Y. Chen (2015), Late Mesoproterozoic to early Neoproterozoic ridge subduction along southern margin of the Jiangnan Orogen: New evidence from the Northeastern Jiangxi Ophiolite (NJO), South China, *Precambrian research*, 268, 1–15, doi: 10.1016/j.precamres.2015.07.005.
- Zhang, F.-Q., Y. Dilek, X.-G. Cheng, H.-X. Wu, X.-B. Lin, and H.-L. Chen (2019), Late Neoproterozoic–early Paleozoic seismic structure–stratigraphy of the SW Tarim Block (China), its passive margin evolution and the Tarim–Rodinia breakup, *Precambrian research*, 334(105456), 105,456, doi: 10.1016/j.precamres.2019.105456.
- Zhao, P., J. He, C. Deng, Y. Chen, and R. N. Mitchell (2021), Early Neoproterozoic (870–820 Ma) amalgamation of the Tarim craton (northwestern China) and the final assembly of Rodinia, *Geology*, 49(11), 1277–1282, doi: 10.1130/g48837.1.
- Zheng, B., W. Zhu, R. Ge, H. Wu, J. He, and Y. Lu (2020), Proterozoic tectonic evolution of the Tarim Craton: New insights from detrital zircon U-Pb and Lu-Hf isotopes of metasediments in the Kuruktag area, *Precambrian research*, 346(105788), 105,788, doi: 10.1016/j.precamres.2020.105788.
- Zhou, T., R. Ge, W. Zhu, and H. Wu (2021), Is there a Grenvillian orogen in the southwestern Tarim Craton?, *Precambrian research*, 354(106053), 106,053, doi: 10.1016/j.precamres.2020.106053.
- Zhou, Y., H. Zhong, W.-G. Zhu, Z.-J. Bai, and C. Li (2022), Neoproterozoic protracted arc basaltic magmatism in the southern margin of the Yangtze Block, south China: New constraints from mafic-ultramafic intrusive rocks, *Precambrian research*, 368(106482), 106,482, doi: 10.1016/j.precamres.2021.106482.
- Zi, J.-W., P. W. Haines, X.-C. Wang, F. Jourdan, B. Rasmussen, G. P. Halverson, S. Sheppard, and C.-F. Li (2019), Pyroxene $^{40}\text{Ar}/^{39}\text{Ar}$ dating of basalt and applications to large igneous provinces and Precambrian stratigraphic correlations, *Journal of geophysical research. Solid earth*, 124(8), 8313–8330, doi: 10.1029/2019jb017713.